© 2015. Published by The Company of Biologists Ltd | Development (2015) 142, 4351-4362 doi:10.1242/dev.129171

RESEARCH ARTICLE

Tropomodulin 1 directly controls thin filament length in both wild-type and tropomodulin 4-deficient skeletal muscle

David S. Gokhin[1,*], Julien Ochala[2], Andrea A. Domenighetti[3,4] and Velia M. Fowler[1,*]

ABSTRACT

The sarcomeric tropomodulin (Tmod) isoforms Tmod1 and Tmod4 cap thin filament pointed ends and functionally interact with the leiomodin (Lmod) isoforms Lmod2 and Lmod3 to control myofibril organization, thin filament lengths, and actomyosin crossbridge formation in skeletal muscle fibers. Here, we show that Tmod4 is more abundant than Tmod1 at both the transcript and protein level in a variety of muscle types, but the relative abundances of sarcomeric Tmods are muscle specific. We then generate *Tmod4*$^{-/-}$ mice, which exhibit normal thin filament lengths, myofibril organization, and skeletal muscle contractile function owing to compensatory upregulation of Tmod1, together with an Lmod isoform switch wherein Lmod3 is downregulated and Lmod2 is upregulated. However, RNAi depletion of Tmod1 from either wild-type or *Tmod4*$^{-/-}$ muscle fibers leads to thin filament elongation by ∼15%. Thus, Tmod1 per se, rather than total sarcomeric Tmod levels, controls thin filament lengths in mouse skeletal muscle, whereas Tmod4 appears to be dispensable for thin filament length regulation. These findings identify Tmod1 as the key direct regulator of thin filament length in skeletal muscle, in both adult muscle homeostasis and in developmentally compensated contexts.

KEY WORDS: Actin filament, Pointed-end capping, Leiomodin, Myofibril, Sarcomere

INTRODUCTION

The semicrystalline arrays of interdigitating, uniform-length actin (thin) and myosin (thick) filaments found in the contracting sarcomeres of skeletal muscle fibers represent a striking example of long-range cytoskeletal organization and precise organelle size control. Whereas thick filament lengths are essentially constant in all skeletal muscles and species examined (∼1.65 µm), thin filament lengths vary substantially across muscles and vertebrate species (0.95-1.40 µm) (Castillo et al., 2009; Gokhin et al., 2012, 2010; Granzier et al., 1991; Ringkob et al., 2004). Thin filament lengths are remarkably plastic during normal postnatal skeletal muscle development and aging (Gokhin et al., 2014a) but can become mis-specified in some congenital myopathies. For example, thin filaments are abnormally short owing to aberrant F-actin assembly and/or destabilization in some nemaline myopathies (Ochala et al., 2012; Ottenheijm et al., 2010, 2009; Yuen et al., 2014), whereas thin filaments elongate as a result of pointed-end uncapping and actin subunit addition in mouse models of Duchenne muscular dystrophy (Gokhin et al., 2014b). Mis-specification of thin filament lengths frequently occurs with alterations in thin filament activation and/or actomyosin crossbridge formation (Chandra et al., 2009; Ochala et al., 2012; Ottenheijm et al., 2013, 2010).

Crucial players in the simultaneous regulation of thin filament lengths, thin filament activation, and actomyosin crossbridge formation are the tropomodulin (Tmod) family of tropomyosin (TM)-binding and actin filament pointed-end capping proteins. Vertebrate skeletal muscles contain two sarcomeric Tmod isoforms: Tmod1, expressed in diverse, terminally differentiated cells, including striated muscle, but also erythrocytes, neurons and ocular lens fiber cells; and Tmod4, which is exclusive to skeletal muscle fibers (Almenar-Queralt et al., 1999; Conley et al., 2001; Gokhin and Fowler, 2011b; Yamashiro et al., 2012). Two sarcomeric Tmod molecules cap each thin filament pointed end and bind to the N-termini of the terminal α/βTM molecules on the thin filaments (Almenar-Queralt et al., 1999; Fowler et al., 1993; Gokhin and Fowler, 2011b; Gokhin et al., 2012, 2010, 2014b). Tmod4 is approximately tenfold more abundant than Tmod1 in a mixture of isolated tibialis anterior (TA) and extensor digitorum longus (EDL) myofibrils (Gokhin et al., 2014b), indicating that Tmod4 is probably the predominant pointed-end cap in skeletal muscle thin filaments, at least in fast muscle. In addition, an extrasarcomeric Tmod isoform, Tmod3, caps the pointed ends of cytoplasmic γ-actin filaments in a sarcoplasmic reticulum (SR)-associated cytoskeletal network (Gokhin and Fowler, 2011a). Skeletal muscle also contains two leiomodin (Lmod) isoforms, Lmod2 and Lmod3, which are larger Tmod family members that nucleate F-actin assembly and can antagonize the capping activity of Tmods (Chereau et al., 2008; Conley et al., 2001; Pappas et al., 2015; Tsukada et al., 2010; Yuen et al., 2014).

Tmod perturbation studies in cultured cardiomyocytes and *Drosophila* indirect flight muscle have demonstrated that sarcomeric Tmods control thin filament lengths by dynamically regulating actin subunit association/dissociation from pointed ends (Bliss et al., 2014; Gregorio et al., 1995; Littlefield et al., 2001; Mardahl-Dumesnil and Fowler, 2001; Sussman et al., 1998) and by stabilizing pointed ends via their interactions with terminal α/βTMs (Mudry et al., 2003). A role for sarcomeric Tmods in regulating thin filament lengths has also been implicated in mammalian skeletal muscle, in which calpain-mediated proteolysis of sarcomeric Tmods in dystrophic muscle is associated with thin filament elongation (Gokhin et al., 2014b), although potential indirect effects due to non-Tmod-related mechanisms have not been ruled out. However, recent analyses of mouse knockouts have uncovered more complex functions of sarcomeric Tmods in mammalian skeletal muscle contractility, as well as unexpected compensatory mechanisms. In *Tmod1*$^{-/-}$ muscle, Tmod3 compensates for the absence of Tmod1 by translocating from its SR compartment to the thin filament pointed ends to preserve normal skeletal muscle development,

[1]Department of Cell and Molecular Biology, The Scripps Research Institute, La Jolla, CA 92037, USA. [2]Centre of Human and Aerospace Physiological Sciences, King's College London, London SE1 1UL, UK. [3]Department of Physical Medicine and Rehabilitation, Feinberg School of Medicine, Northwestern University, Chicago, IL 60611, USA. [4]Rehabilitation Institute of Chicago, Chicago, IL 60611, USA.

*Authors for correspondence (dgokhin@scripps.edu; velia@scripps.edu)

Received 29 July 2015; Accepted 5 November 2015

Development (2015) 142, 4351-4362 doi:10.1242/dev.129171

myofibril assembly and thin filament lengths (Gokhin and Fowler, 2011a; Gokhin et al., 2010). The switch from pointed-end capping by Tmod1 and Tmod4 in wild-type muscle to pointed-end capping by Tmod3 and Tmod4 in *Tmod1*$^{-/-}$ muscle impairs initial α/βTM movement during thin filament activation, inhibiting the formation of productive actomyosin crossbridges and depressing isometric force production (Ochala et al., 2014).

Although analyses of dystrophic and *Tmod1*$^{-/-}$ skeletal muscles have provided substantial insights into how sarcomeric Tmods regulate thin filament lengths and muscle physiology, direct evidence for Tmod-mediated regulation of skeletal muscle thin filament lengths has not been found. Additionally, the approximately tenfold greater abundance of Tmod4 than Tmod1 in TA and EDL myofibrils (Gokhin et al., 2014b) led us to hypothesize that the properties of Tmod4 at pointed ends are distinct from those of Tmod1. Here, we report that Tmod4 is more abundant than Tmod1 at both the transcript and protein level in both fast- and slow-switch muscles, but molar ratios of sarcomeric Tmods are muscle specific. We then generated a novel *Tmod4*$^{-/-}$ mouse and unexpectedly discovered that *Tmod4*$^{-/-}$ muscles exhibit normal thin filament lengths and contractile function owing to compensatory upregulation of Tmod1, with accompanying downregulation of Lmod3 and upregulation of Lmod2. RNAi depletion of Tmod1 from either wild-type or *Tmod4*$^{-/-}$ muscles leads to actin subunit addition onto pointed ends and identical extents of thin filament elongation, indicating that Tmod1 and not Tmod4 is required for thin filament length regulation in mouse skeletal muscles. These findings demonstrate that pointed-end capping by sarcomeric Tmods directly controls thin filament lengths in both adult muscle homeostasis and in developmentally compensated contexts.

RESULTS

Gene expression and protein abundance of sarcomeric Tmods

To determine whether the relative abundances of Tmod4 and Tmod1 are fixed or variable across muscle types, we performed quantitative western blotting of diverse skeletal muscles (TA, soleus and diaphragm) lysates and determined the molar ratio of sarcomeric Tmods in each muscle. Tmod4 was more abundant than Tmod1 in all muscles examined, but Tmod4 ranged from approximately nine- to tenfold more abundant than Tmod1 in TA, approximately fourfold more abundant in soleus, and approximately threefold more abundant in diaphragm (Table 1), indicating that sarcomeric Tmod isoform distributions are muscle type dependent. In all muscles, approximately two sarcomeric Tmods were associated with each thin filament pointed end (Table 1), as observed previously (Gokhin et al., 2014b). Note that the higher Tmod1 levels observed in soleus and diaphragm muscles (Table 1) might be due to the heavier vascularization of these muscles and the presence of Tmod1-containing erythrocytes (Moyer et al., 2010). However, this is unlikely, as we do not observe noteworthy differences in Tmod1 abundances in isolated myofibrils versus whole-muscle lysates (compare Table 1 and data published by Gokhin et al., 2014b). Alternatively, slow muscles such as the soleus and diaphragm might contain more extrasarcomeric Tmod1 than do fast muscles, possibly associated with the SR or T-tubules (Gokhin and Fowler, 2011a), leading to higher total Tmod1 levels.

Next, to determine whether the greater abundance of Tmod4 compared with Tmod1 in various skeletal muscles could be explained by differences in gene expression, we analyzed the expression of Tmod genes in diverse striated muscles [TA, soleus, diaphragm and cardiac left ventricle (LV)] using RNA-seq. *Tmod4* mRNA was more abundant than *Tmod1* mRNA in TA, soleus and diaphragm (Fig. 1A), consistent with the higher levels of Tmod4 protein in these muscles (Table 1); this observation was confirmed by qRT-PCR (Fig. 1B). By contrast, *Tmod1* mRNA was more abundant than *Tmod4* mRNA in LV (Fig. 1A), as expected (Gokhin and Fowler, 2011b). Therefore, muscle-specific molar ratios of Tmod4:Tmod1 proteins correlate with mRNA levels.

To complete our survey of Tmod family gene expression, we examined the expression of nonsarcomeric Tmod genes, as well as Lmod genes. Expression of *Tmod3* mRNA was low but above background in all striated muscles examined (Fig. 1A), consistent with Tmod3's SR association with γ_{cyto}-actin (Gokhin and Fowler, 2011a), an actin isoform that is ∼1/4000th as abundant as the α_{sk}-actin that comprises the thin filaments (Hanft et al., 2006). *Lmod2*

Table 1. Stoichiometry of sarcomeric Tmods associated with thin filaments in diverse mouse muscles

	Amount of Tmod1 (ng/µl)* in gel sample	Amount of Tmod4 (ng/µl)* in gel sample*	Amount of actin (ng/µl)‡ in gel sample	Amount of Tmod4 (mol) per mole Tmod1	Amount of actin (mol) per mole sarcomeric Tmods	Number of sarcomeric Tmods per thin filament§
TA						
Expt. 1	0.44±0.09	4.19±0.37	980±48	9.6	210	1.9
Expt. 2	0.53±0.09	4.77±0.30	1044±112	9.0	197	2.0
Expt. 3	0.42±0.17	4.25±0.34	1017±98	10.1	218	1.8
Soleus						
Expt. 1	0.89±0.28	3.46±0.45	962±69	3.9	221	1.9
Expt. 2	0.74±0.16	3.34±0.52	1040±126	4.5	198	2.2
Expt. 3	1.05±0.13	4.02±0.29	936±46	4.0	238	1.8
Diaphragm						
Expt. 1	1.33±0.35	4.21±0.33	1035±105	3.2	214	2.0
Expt. 2	1.48±0.39	4.47±0.54	1127±132	3.1	189	2.3
Expt. 3	1.50±0.42	4.39±0.51	1070±163	2.9	191	2.2

*Amounts of sarcomeric Tmods were determined by quantitative western blotting and densitometry of skeletal muscle myofibrils (1-8 µl gel sample) electrophoresed alongside purified recombinant protein standards (0.25-4 ng) on the same gel. Tmod1 or Tmod4 protein standards were mixed with *Tmod1*$^{-/-}$ or *Tmod4*$^{-/-}$ TA muscle lysates, respectively, to equalize the effects of endogenous non-Tmod proteins on the western transfer efficiencies of endogenous versus recombinant purified Tmods. Standard deviations reflect three to four different myofibril volumes from different lanes on the same blot.

‡Amounts of actin were determined by densitometry of Coomassie Blue-stained gels containing skeletal muscle myofibrils (1-8 µl gel sample) electrophoresed alongside rabbit skeletal muscle actin standards (0.25-4 µg) on the same gel. Standard deviations reflect three to four different myofibril volumes from different lanes on the same gel.

§Numbers of Tmods/thin filament were calculated based on 13 actin subunits per 37 nm of thin filament (Fowler et al., 1993).

Development (2015) 142, 4351-4362 doi:10.1242/dev.129171

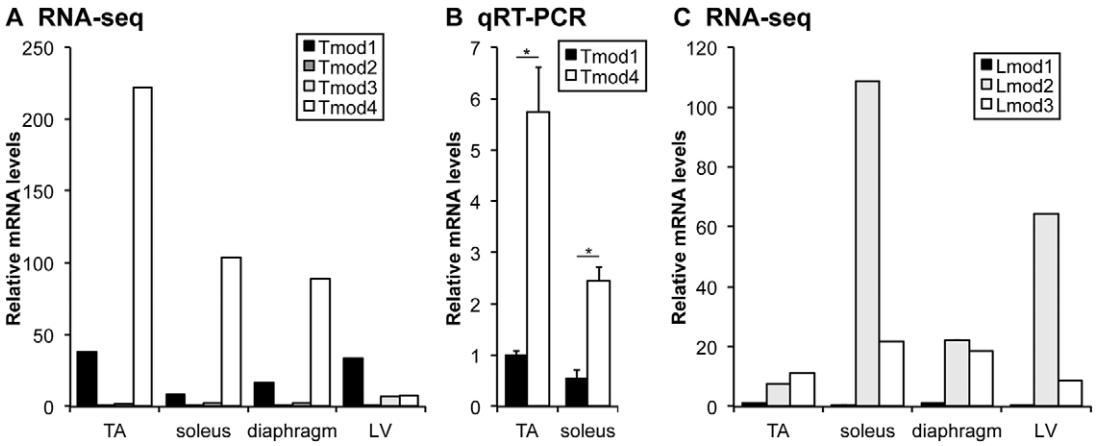

Fig. 1. Gene expression of Tmod family members in striated muscles. (A) Expression of *Tmod1-4* mRNAs in TA, soleus, diaphragm and LV muscle determined by RNA-seq. (B) Expression of *Tmod1* and *Tmod4* mRNAs in TA and soleus muscles determined by qRT-PCR. Error bars reflect mean±s.e.m. of n=3 replicates. *P<0.05. (C) Expression of *Lmod1-3* mRNAs in TA, soleus, diaphragm and LV muscle determined by RNA-seq. For RNA-seq analyses, three individual muscles of each type were pooled, and RNA-seq analysis was performed on the pooled sample; hence, no error bars are shown.

and *Lmod3* mRNAs were detected in all striated muscles, in agreement with previous studies (Cenik et al., 2015; Chereau et al., 2008; Conley et al., 2001; Nworu et al., 2015; Tian et al., 2015; Yuen et al., 2014), but an unexpected muscle type dependence was observed, with *Lmod2* mRNA predominating in slow-twitch soleus, diaphragm, and left ventricular muscles and *Lmod3* mRNA more highly expressed than *Lmod2* mRNA in fast-twitch TA muscle (Fig. 1C). *Tmod2* and *Lmod1* mRNAs were not detected in striated muscles (Fig. 1A,C), consistent with *Tmod2* expression being restricted to neuronal tissues (Cox et al., 2003; Watakabe et al., 1996) and *Lmod1* expression being restricted to smooth muscle (Conley et al., 2001; Nanda and Miano, 2012).

Deletion of Tmod4 induces compensatory upregulation of Tmod1 to maintain normal myofibril organization, thin filament lengths and muscle function

Because Tmod4, and not Tmod1, is the predominant sarcomeric Tmod isoform in mouse skeletal muscles (Table 1), we explored the effects of Tmod4 deficiency in mice by generating $Tmod4^{-/-}$ mice, which lack Tmod4 protein in skeletal muscle (Fig. 2A-C). Surprisingly, $Tmod4^{-/-}$ mice were born in Mendelian ratios and were viable and fertile, with no overt myopathy, identical to $Tmod4^{+/+}$ and $Tmod4^{+/-}$ mice. TA, EDL and soleus muscles from $Tmod4^{-/-}$ mice exhibited no abnormalities in terms of centralized nuclei (Fig. 2D,E), fiber cross-sectional area (Fig. 2F), MHC distribution (Fig. 2G), myofibrillar ultrastructure (Fig. 2H) and physiological parameters (Fig. 2I-L). Immunostaining for α-actinin and phalloidin staining for F-actin confirmed normal organization of striated arrays of Z-lines and thin filaments in $Tmod4^{-/-}$ muscles (Fig. 3A). Thus, Tmod4 appears to be dispensable for myofibril organization and skeletal muscle function in mice.

To test whether Tmod1 and/or Tmod3 could compensate for the absence of Tmod4 in $Tmod4^{-/-}$ mice, we immunostained longitudinal cryosections of $Tmod4^{+/+}$ and $Tmod4^{-/-}$ muscles for Tmod1 and Tmod3. In both $Tmod4^{+/+}$ and $Tmod4^{-/-}$ muscles, Tmod1 exhibited its familiar striated staining pattern of periodic doublets, corresponding to the pointed ends of phalloidin-stained thin filaments, but the fluorescence intensity of Tmod1 was qualitatively brighter in $Tmod4^{-/-}$ muscles, suggesting higher levels of Tmod1 (Fig. 3B; Fig. S1A). This was confirmed by western blotting, which showed approximately six- to eightfold increases in Tmod1 protein levels in $Tmod4^{-/-}$ muscles (Fig. 3D,E), which was driven by approximately five- to sixfold increases in *Tmod1* gene expression (Fig. 3F). Thus, the increased Tmod1 repopulated most of the pointed ends rendered vacant by the absence of Tmod4 (Table 1; Fig. 3H). Similar compensatory increases in Tmod1 protein levels were observed in leg and flank muscles from newborn (P0) $Tmod4^{-/-}$ mice (Fig. S2), indicating that compensatory elevation of Tmod1 levels occurs sometime during embryonic skeletal muscle development of $Tmod4^{-/-}$ mice and does not require postnatal muscle contractility and use. Unlike Tmod1, Tmod3 localized predominantly to Z-line-flanking puncta and to a lesser extent to M-line puncta in both $Tmod4^{+/+}$ and $Tmod4^{-/-}$ muscles (Fig. 3C; Fig. S1B), indicative of the SR localization of Tmod3 (Gokhin and Fowler, 2011a), but protein levels of Tmod3 were unchanged in $Tmod4^{-/-}$ muscles (Fig. 3D,E). Therefore, Tmod1 compensates for the absence of Tmod4 via an increase in protein levels. This compensation mechanism differs from that of $Tmod1^{-/-}$ muscle, wherein Tmod3 compensates for the absence of Tmod1 via translocation from the SR and no change in protein levels (Gokhin and Fowler, 2011a; Gokhin et al., 2010). However, this compensation mechanism resembles that of $Tmod2^{-/-}$ brain, wherein Tmod1 protein levels are increased approximately eightfold to compensate for the absence of Tmod2 in neurons (Cox et al., 2003).

Next, we investigated whether the switch from Tmod1/Tmod4 pointed-end capping in $Tmod4^{+/+}$ muscle to exclusively Tmod1 pointed-end capping in $Tmod4^{-/-}$ muscle might alter thin filament lengths. Hence, we performed distributed deconvolution (DDecon) analysis of line-scans from fluorescence images to measure thin filament lengths based on distances of sarcomeric Tmods from the Z-line as well as by breadths of the F-actin striations (Gokhin and Fowler, 2013; Littlefield and Fowler, 2002). In both $Tmod4^{+/+}$ and $Tmod4^{-/-}$ TA muscles, thin filament lengths were ∼1.07 µm determined by Tmod distance and ∼0.99 µm determined by F-actin breadth (Fig. 3G), in agreement with previous studies (Gokhin et al., 2010, 2014b). In both $Tmod4^{+/+}$ and $Tmod4^{-/-}$ soleus muscles, thin filament lengths were ∼1.18 µm determined by Tmod distance and ∼1.10 µm determined by F-actin breadth (Fig. 3G). Therefore, compensatory upregulation of Tmod1 preserves normal thin filament lengths in $Tmod4^{-/-}$ muscle (Fig. 3H).

In skeletal muscle, thin filament lengths are stabilized by nebulin, a giant protein that co-extends with thin filaments, protects thin filaments from depolymerization and shortening, and attenuates

Development (2015) 142, 4351-4362 doi:10.1242/dev.129171

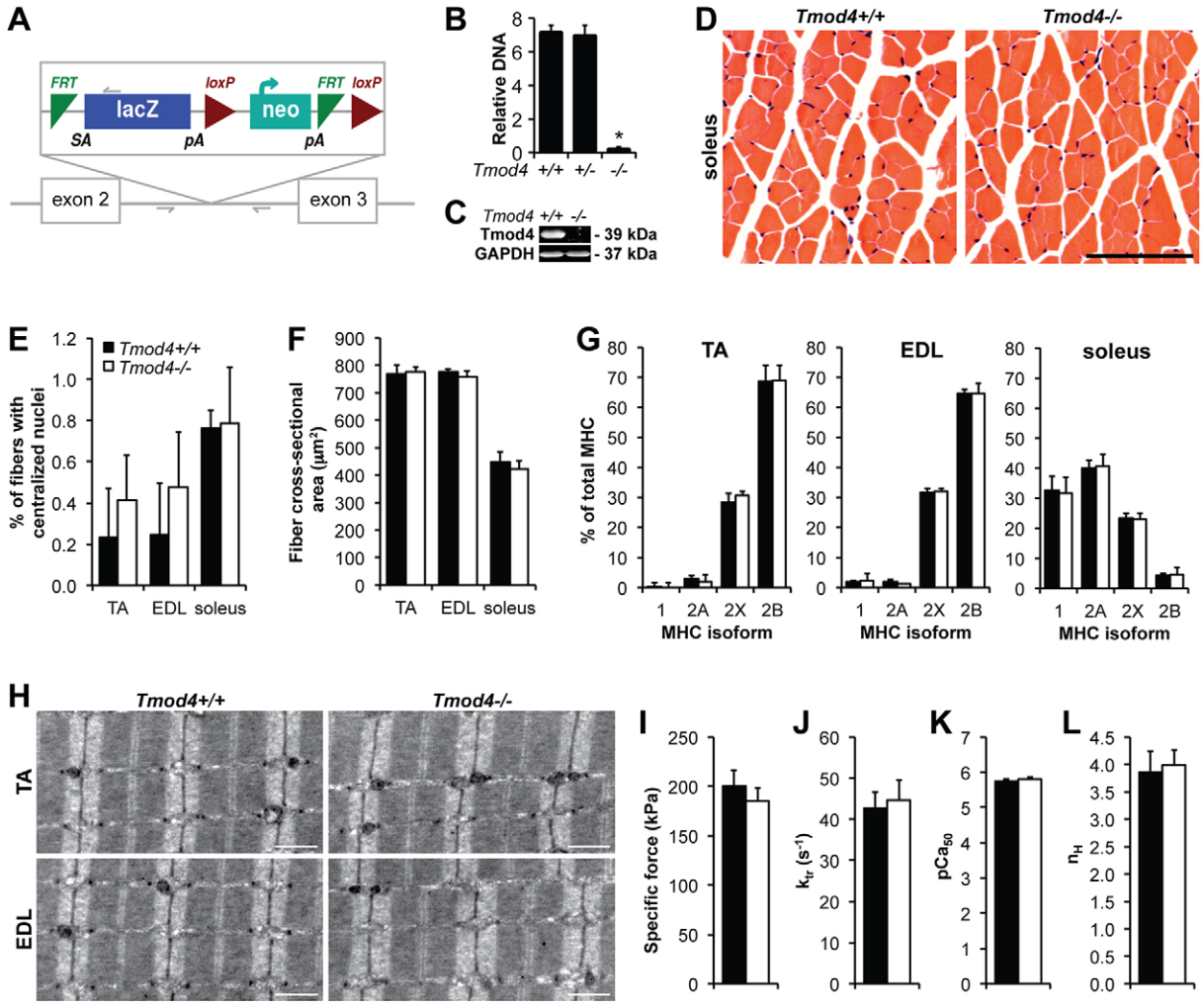

Fig. 2. Deletion of Tmod4 does not produce an overt myopathic phenotype. (A) *Tmod4* gene targeting strategy generated by KOMP, depicting *lacZ*/*neo* insertion into intron 2 of *Tmod4*. (B) Automated qPCR analysis of genomic DNA from mouse tail-snip biopsies derived from $Tmod4^{+/-}$ intercrosses. *P<0.001 versus other groups. (C) Western blots of homogenates of TA muscles from 2-month-old $Tmod4^{+/+}$ and $Tmod4^{-/-}$ mice probed using an anti-Tmod4 antibody. Gapdh was used as a loading control. (D) H&E-stained cross-sections of soleus muscles from 2-month-old $Tmod4^{+/+}$ and $Tmod4^{-/-}$ mice. Scale bar: 300 µm. (E,F) Histological evaluation of centralized nuclei (E) and fiber cross-sectional area (F) in TA, EDL and soleus muscles from 2-month-old $Tmod4^{+/+}$ and $Tmod4^{-/-}$ mice. Error bars reflect mean±s.e.m. of n=4 muscles/genotype. (G) Evaluation of MHC isoform distributions in TA, EDL and soleus muscles from 2-month-old $Tmod4^{+/+}$ and $Tmod4^{-/-}$ mice using 8% SDS-PAGE followed by silver staining and densitometric quantification. Error bars reflect mean±s.e.m. of n=4 muscles/genotype. (H) Representative TEM micrographs of longitudinal sections of TA and EDL muscles from 2-month-old $Tmod4^{+/+}$ and $Tmod4^{-/-}$ mice. Scale bars: 1 µm. (I-L) Physiological evaluation of skinned, Ca^{2+}-activated muscle fibers from TA muscles from 2-month-old $Tmod4^{+/+}$ and $Tmod4^{-/-}$ mice. Shown are specific force production (I), crossbridge cycling kinetics as determined by the rate constant of force redevelopment after unloaded sarcomere shortening (k_{tr}; J), thin filament Ca^{2+} sensitivity (pCa_{50}; K), and cooperativity of thin filament activation [Hill coefficient (n_H); L]. Error bars reflect mean±s.e.m. of n=8 fibers/genotype.

actin and Tmod dynamics at the pointed end (Bang et al., 2006; Pappas et al., 2011, 2010). Nebulin extends from its C-terminus (neb-C) anchored in the Z-line to its N-terminal M1M2M3 domain (neb-N) located at a constant distance from the Z-line (~0.95 µm), slightly proximal to the pointed ends where sarcomeric Tmods are located (Gokhin and Fowler, 2013). Because nebulin and sarcomeric Tmods are thought to collaboratively regulate thin filament lengths, we investigated whether deletion of Tmod4 might impact the assembly or localization of nebulin. To test this, we immunostained longitudinal cryosections of $Tmod4^{+/+}$ and $Tmod4^{-/-}$ muscles for neb-N and neb-C. In both $Tmod4^{+/+}$ and $Tmod4^{-/-}$ muscles, neb-N localized to striations slightly proximal to the thin filament pointed ends (Fig. 4A), as expected (Gokhin and Fowler, 2013), whereas neb-C precisely colocalized with α-actinin in the Z-line (Fig. 4B), also as expected (Pappas et al., 2008, 2010). The neb-N striations in both TA and soleus muscles from $Tmod4^{+/+}$ and $Tmod4^{-/-}$ mice were ~0.95 µm from the Z-line, as confirmed by DDecon analysis (Fig. 4D). Therefore, deletion of Tmod4 does not impact nebulin localization.

Deletion of Tmod4 alters the expression of striated muscle Lmod isoforms

Tmod4 has been proposed to interact functionally with the actin nucleator Lmod3 near the thin filament pointed ends, based on a dramatic decrease in Tmod4 protein levels in Lmod3-deficient nemaline myopathy patients (Yuen et al., 2014) and the ability of Tmod4 and Lmod3 to substitute for one another during skeletal myofibril assembly in *Xenopus* (Nworu et al., 2015). To evaluate this functional interaction, we examined whether deletion of Tmod4 might impact the localization or levels of Lmod3. In both $Tmod4^{+/+}$

Development (2015) 142, 4351-4362 doi:10.1242/dev.129171

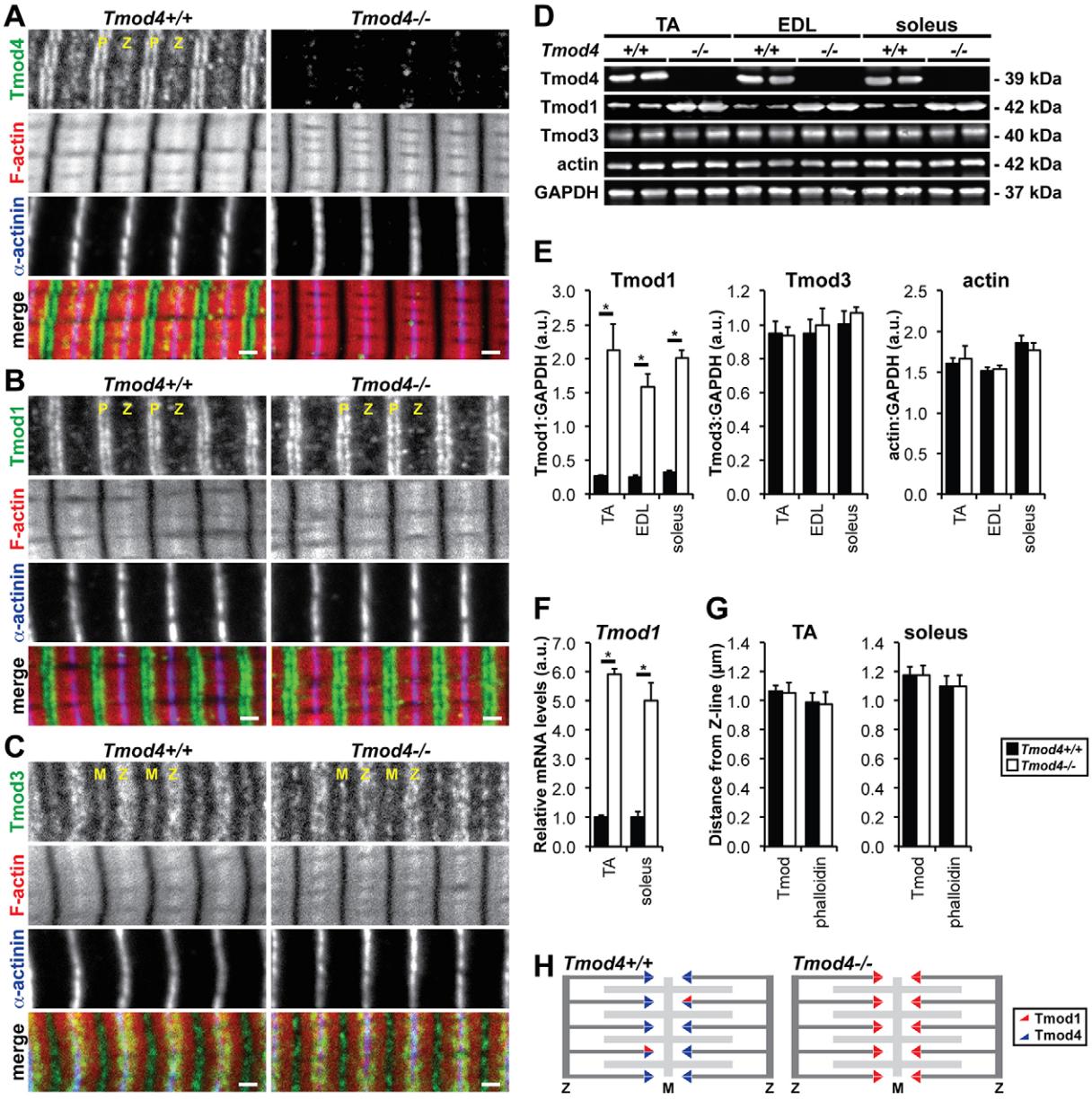

Fig. 3. Deletion of Tmod4 induces compensatory upregulation of Tmod1 to preserve myofibril organization and thin filament lengths. (A-C) Longitudinal cryosections of TA muscles from 2-month-old *Tmod4*$^{+/+}$ and *Tmod4*$^{-/-}$ mice were immunostained for Tmod4 (A), Tmod1 (B) or Tmod3 (C), immunostained for α-actinin, and phalloidin-stained for F-actin. M, M-line; P, thin filament pointed ends; Z, Z-line. Scale bars: 1 μm. (D) Western blots of homogenates of TA, EDL and soleus muscles from 2-month-old *Tmod4*$^{+/+}$ and *Tmod4*$^{-/-}$ mice were probed using antibodies against Tmod4, Tmod1, Tmod3 and actin. Gapdh was used as a loading control. (E) Quantification of western blots. Error bars reflect mean±s.e.m. of *n*=4 lanes/genotype within a single blot. **P*<0.05. (F) Expression of *Tmod1* mRNA in TA and soleus muscles from *Tmod4*$^{+/+}$ and *Tmod4*$^{-/-}$ mice determined by qRT-PCR. Error bars reflect mean±s.e.m. of *n*=3 replicates. **P*<0.05. (G) Thin filament lengths in TA and soleus muscles from 2-month-old *Tmod4*$^{+/+}$ and *Tmod4*$^{-/-}$ mice determined using DDecon analysis of fluorescence images. Parameters correspond to the breadth of phalloidin staining and the distances of Tmod and nebulin M1M2M3 from the Z-line. In *Tmod4*$^{+/+}$ muscle, Tmod lengths were determined from both Tmod1 and Tmod4 immunostaining. In *Tmod4*$^{-/-}$ muscle, Tmod lengths were determined from only Tmod1 immunostaining. Error bars reflect mean±s.d. of *n*=50 myofibrils/genotype randomly selected from *n*=4 muscles/genotype. (H) Possible model of sarcomeric Tmod isoform association with thin filament pointed ends in sarcomeres from *Tmod4*$^{+/+}$ and *Tmod4*$^{-/-}$ muscles.

and *Tmod4*$^{-/-}$ muscles, Lmod3 localized to striations at or near the thin filament pointed ends (Fig. 4C), as expected (Nworu et al., 2015; Yuen et al., 2014). The Lmod3 striations were ∼0.95 μm from the Z-line (Fig. 4D), coincident with neb-N and not the thin filament pointed end where Tmods are located (compare with Fig. 3G). We were also unable to detect Tmod-Lmod associations by co-immunoprecipitation (Fig. S3).

Surprisingly, western blotting of *Tmod4*$^{-/-}$ muscle lysates revealed a ∼60% decrease in Lmod3 protein levels, with a corresponding increase in Lmod2 (Fig. 4E,F). These changes in Lmod isoform levels are due to corresponding changes in *Lmod3* and *Lmod2* mRNA levels (Fig. 4G). Therefore, the switch from Tmod1/Tmod4 pointed-end capping in *Tmod4*$^{+/+}$ muscle to solely Tmod1 pointed-end capping in *Tmod4*$^{-/-}$ muscle shifts Lmod isoform abundance away from Lmod3 and towards Lmod2. However, as Tmods neither colocalize nor co-immunoprecipitate with Lmods, preferential Tmod4/Lmod3 and Tmod1/Lmod2 co-expression is unlikely to be regulated at the level of a protein

Development (2015) 142, 4351-4362 doi:10.1242/dev.129171

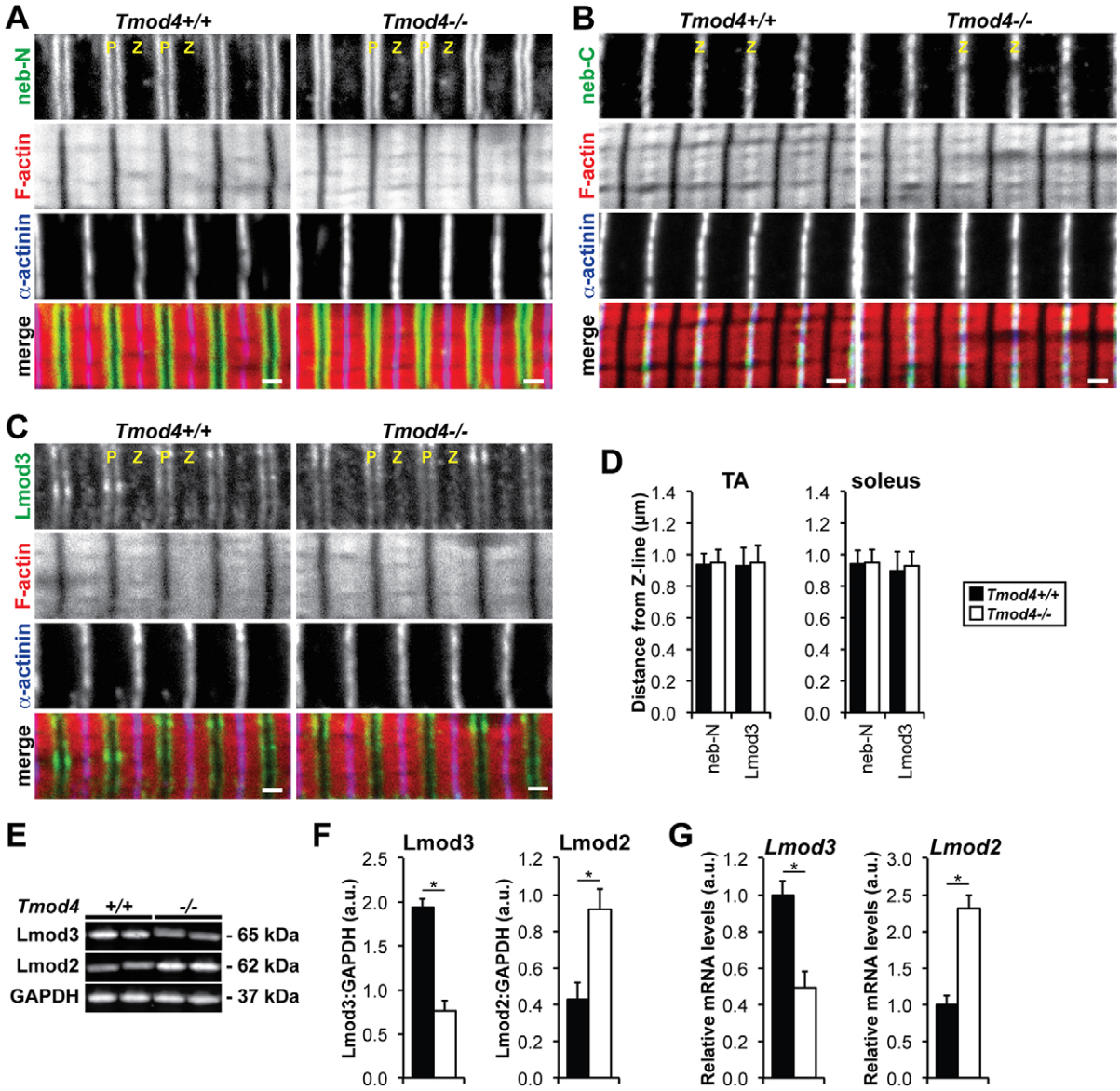

Fig. 4. Deletion of Tmod4 induces downregulation of Lmod3 with concomitant upregulation of Lmod2, but does not impact the localization of nebulin. (A-C) Longitudinal cryosections of TA muscles from 2-month-old *Tmod4*$^{+/+}$ and *Tmod4*$^{-/-}$ mice were immunostained for neb-N (A), neb-C (B) or Lmod3 (C), immunostained for α-actinin, and phalloidin-stained for F-actin. P, thin filament pointed ends; Z, Z-line. Scale bars: 1 μm. (D) Distances of neb-N and Lmod3 from the Z-line in TA and soleus muscles from 2-month-old *Tmod4*$^{+/+}$ and *Tmod4*$^{-/-}$ mice determined using DDecon analysis of fluorescence images. Error bars reflect mean±s.d. of *n*=50 myofibrils/genotype randomly selected from *n*=4 muscles/genotype. (E) Western blots of homogenates of TA muscles from 2-month-old *Tmod4*$^{+/+}$ and *Tmod4*$^{-/-}$ mice were probed using antibodies against Lmod3 and Lmod2. Gapdh was used as a loading control. (F) Quantification of western blots. Error bars reflect mean±s.e.m. of *n*=4 lanes/genotype within a single blot. **P*<0.05. (G) Expression of *Lmod3* and *Lmod2* mRNA in TA muscles from *Tmod4*$^{+/+}$ and *Tmod4*$^{-/-}$ mice determined by qRT-PCR. Error bars reflect mean±s.e.m. of *n*=3 replicates. **P*<0.05.

complex; instead, Tmod4/Lmod3 versus Tmod1/Lmod2 co-expression might be mediated by a gene regulatory network, like other combinations of muscle cytoskeletal protein isoforms (Olson and Nordheim, 2010; Schiaffino and Reggiani, 1996).

Depletion of Tmod1 from wild-type or Tmod4-deficient muscles results in increased thin filament lengths

A direct role for sarcomeric Tmods in regulating thin filament length in mammalian skeletal muscle has remained elusive, owing to developmental compensation by other Tmod isoforms in *Tmod1*$^{-/-}$ and *Tmod4*$^{-/-}$ muscles (Fig. 3; Gokhin and Fowler, 2011a; Gokhin et al., 2010). To overcome this, we depleted Tmod1 from adult muscles using *in vivo* RNAi, in which we injected *Tmod4*$^{+/+}$ and *Tmod4*$^{-/-}$ TA muscles with either negative-control siRNA (siScr) or one of two *Tmod1*-targeting siRNAs (siTmod1a and siTmod1b). Muscle fibers from siScr-injected TA muscles consistently exhibited striated Tmod1 staining, whereas fibers from siTmod1a- and siTmod1b-injected muscles showed widespread loss of striated Tmod1 staining in many fibers (Fig. 5A,B; Fig. S4). The extent of knockdown was quantified as the percentage of fibers with striated Tmod1 staining, which was ∼100% for siScr-injected TA muscles but reduced to ∼25-50% for siTmod1a- and siTmod1b-injected muscles (Fig. 5C). The effects of siTmod1a and siTmod1b injection were similar in *Tmod4*$^{+/+}$ and *Tmod4*$^{-/-}$ muscles (Fig. 5A-C), despite substantially higher *Tmod1* mRNA levels and Tmod1 protein levels in *Tmod4*$^{-/-}$ muscles prior to

Development (2015) 142, 4351-4362 doi:10.1242/dev.129171

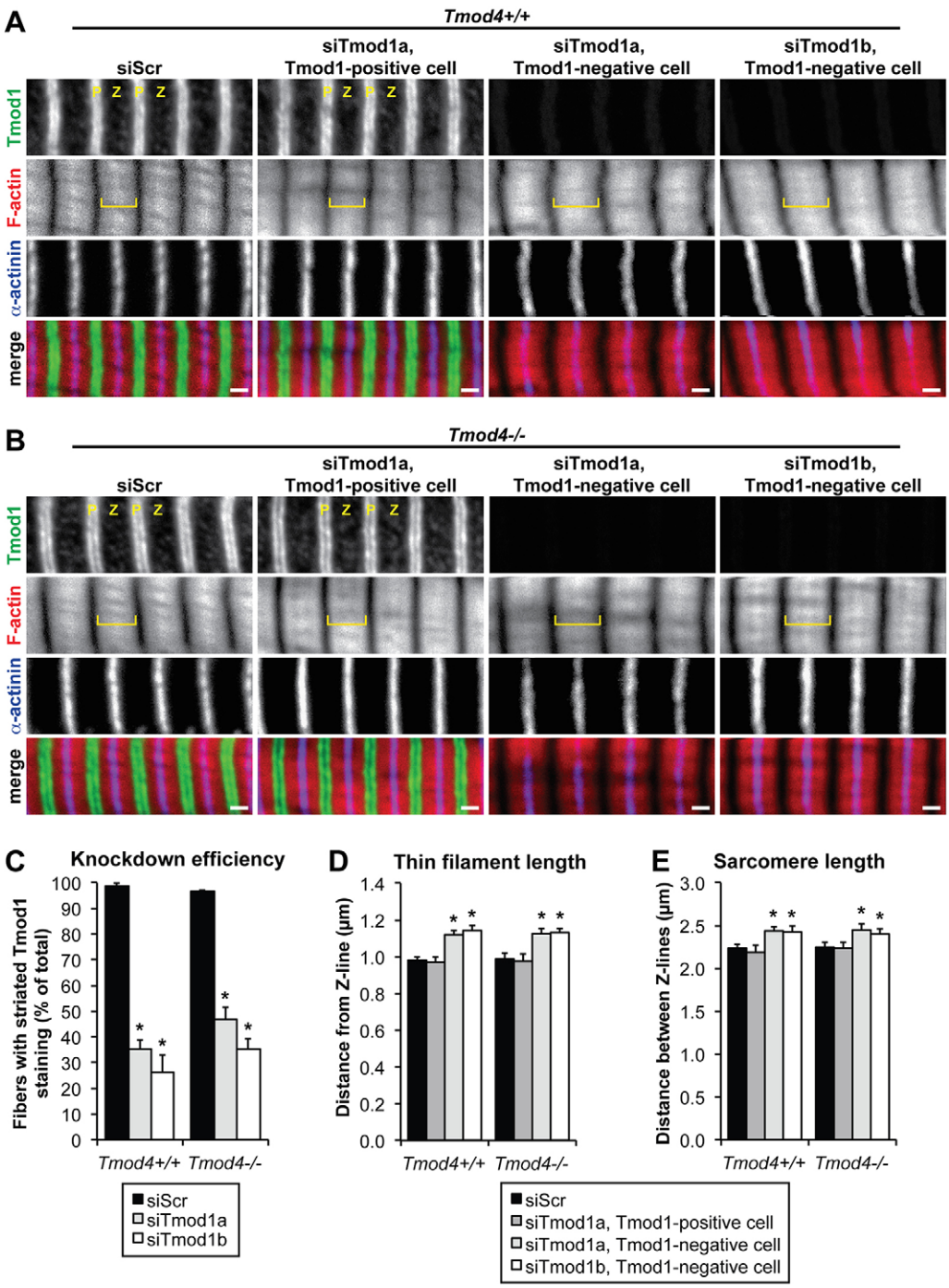

Fig. 5. RNAi knockdown of Tmod1 from *Tmod4*$^{+/+}$ or *Tmod4*$^{-/-}$ muscles leads to increased thin filament lengths. (A,B) TA muscles from 2-month-old *Tmod4*$^{+/+}$ (A) and *Tmod4*$^{-/-}$ (B) mice were injected with siScr, siTmod1a or siTmod1b and excised 1 week post-injection. Shown are longitudinal cryosections immunostained for Tmod1 and α-actinin, and phalloidin-stained for F-actin. For siTmod1a, images of a muscle fiber away from the siRNA injection site ('Tmod1-positive cell') are also shown, serving as an internal control. Yellow brackets signify thin filament arrays (I-Z-I regions) that widen after Tmod1 knockdown. P, thin filament pointed ends; Z, Z-line. Scale bars: 1 μm. (C) Extent of Tmod1 knockdown as measured by the percentage of fibers with striated Tmod1 immunostaining in TA muscles injected with siScr, siTmod1a or siTmod1b. Error bars reflect mean±s.e.m. of *n*=3-4 muscles. (D,E) Measurement of thin filament lengths (D) and sarcomere lengths (E) in TA muscles at maximal plantarflexion in 2-month-old *Tmod4*$^{+/+}$ and *Tmod4*$^{-/-}$ mice injected with siScr, siTmod1a or siTmod1b, determined using DDecon analysis of fluorescence images. Error bars reflect mean±s.d. of *n*=50 myofibrils/genotype randomly selected from *n*=3-4 muscles/genotype. **P*<0.01 versus siScr.

injection (Fig. 3). Tmod3 remained localized to Z-line-flanking and M-line puncta in siTmod1a- and siTmod1b-injected muscles (Fig. S5A,B), indicating that siRNA knockdown of Tmod1 does not induce compensatory translocation of Tmod3 from the SR to the thin filament pointed ends, as observed in *Tmod1*$^{-/-}$ muscle (Gokhin and Fowler, 2011a; Gokhin et al., 2010).

Tmod1-negative fibers in siTmod1a- and siTmod1b-injected TA muscles exhibited a wider breadth of sarcomeric F-actin staining, indicative of increased thin filament lengths (Fig. 5A,B, yellow brackets). Indeed, thin filament lengths in Tmod1-positive fibers were ∼0.98 μm, whereas thin filament lengths in Tmod1-negative knockdown fibers increased to ∼1.13 μm (Fig. 5D). This ∼15% increase is slightly greater than the ∼10% increase observed in dystrophic TA muscles exhibiting m-calpain-mediated proteolysis of Tmod1 (Gokhin et al., 2014b), suggesting that residual unproteolyzed Tmod1 remaining in dystrophic TA muscle might still confer partial length-regulating activity. Neb-N remained normally localized at ∼0.95 μm from the Z-line in siTmod1a- and siTmod1b-injected muscles (Fig. S5C-E), indicating that overall thin filament elongation was driven specifically by elongation of the nebulin-free distal segment and not the nebulin-coated proximal segment (Gokhin and Fowler, 2013). Depletion of Tmod1 from *Tmod4*$^{+/+}$ fibers did not affect variability of thin filament lengths (Fig. 5D; data not shown), even though the abundance of Tmod1 indicates that it caps just a subset (∼10%) of thin filaments (Table 1). Notably, Tmod4 remained normally localized at the

Development (2015) 142, 4351-4362 doi:10.1242/dev.129171

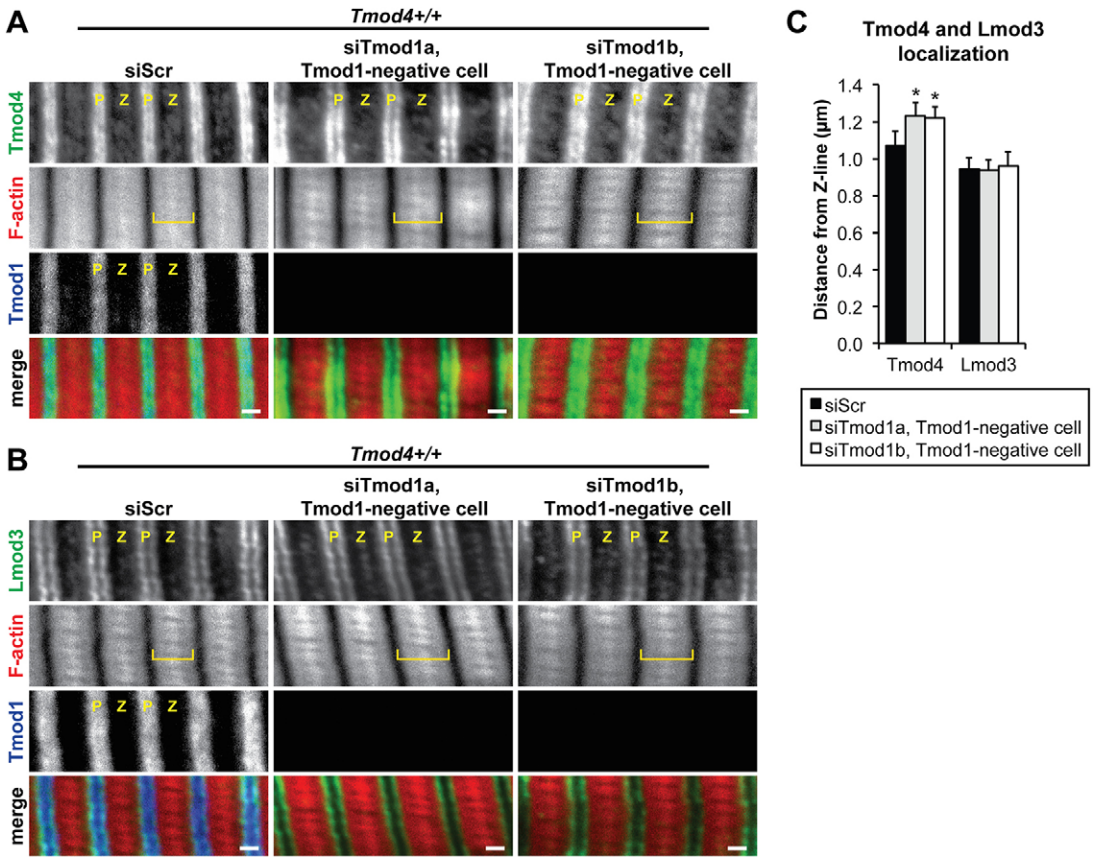

Fig. 6. RNAi knockdown of Tmod1 from wild-type muscle does not alter the localization of Tmod4 or Lmod3. (A,B) TA muscles from 2-month-old *Tmod4*$^{+/+}$ mice were injected with siScr, siTmod1a or siTmod1b and excised 1 week post-injection. Shown are longitudinal cryosections immunostained for Tmod1 and either Tmod4 (A) or Lmod3 (B), and phalloidin-stained for F-actin. Yellow brackets signify thin filament arrays (I-Z-I regions) that widen after Tmod1 knockdown. P, thin filament pointed ends; Z, Z-line. Scale bars: 1 µm. (C) Distances of Tmod4 and Lmod3 from the Z-line in TA muscles from 2-month-old *Tmod4*$^{+/+}$ mice injected with siScr, siTmod1a or siTmod1b, determined using DDecon analysis of fluorescence images. Error bars reflect mean±s.d. of *n*=50 myofibrils/genotype randomly selected from *n*=3-4 muscles/genotype. **P*<0.01 versus siScr.

pointed ends of the elongated thin filaments in siTmod1a- and siTmod1b-injected *Tmod4*$^{+/+}$ muscles (Fig. 6A,C), indicating that Tmod4 acts as a dynamic cap, similar to Tmod1 (Gregorio et al., 1995; Littlefield et al., 2001). Moreover, Lmod3 remained ∼0.95 µm from the Z-line in siTmod1a- and siTmod1b-injected *Tmod4*$^{+/+}$ muscles (Fig. 6B,C), coincident with Neb-N (Fig. S5C-E), indicating that Lmod3 does not translocate to the pointed end to promote thin filament elongation in the absence of Tmod1.

Increased thin filament lengths in Tmod1-negative fibers were associated with increased sarcomere lengths at an ankle joint angle corresponding to maximal plantar flexion (Fig. 5E), suggesting that thin filament elongation drives sarcomere growth by inducing longitudinal separation of successive Z-lines. Coordination of thin filament length with sarcomere length has been observed during growth of *Drosophila* indirect flight muscle (Mardahl-Dumesnil and Fowler, 2001) but the relevance of this to mammalian muscle is unclear (Littlefield and Fowler, 2008). It remains unknown whether thin filament elongation might drive sarcomere length changes during mammalian muscle development, and whether thin filament length changes might underlie sarcomere length changes under conditions of muscle adaptation and remodeling (Lieber, 2002).

DISCUSSION

Here, we show that Tmod4 is the predominant sarcomeric Tmod at both the transcript and protein level in both fast and slow skeletal muscles, but Tmod4:Tmod1 ratios are muscle specific. Muscle-specific sarcomeric Tmod isoform distributions represent a novel, myofibril-intrinsic signature of muscle types, similar to MHC, α/βTM and troponin isoform distributions and Z-line widths (Pette and Staron, 1990). Although Tmod4 is the predominant Tmod in all muscles examined, deletion of Tmod4 does not produce an overt myopathy, as normal myofibril organization, thin filament lengths, and actomyosin contractile function are observed in *Tmod4*$^{-/-}$ skeletal muscle. This is probably due to the compensatory upregulation of Tmod1 being of sufficient magnitude to repopulate nearly all the thin filament pointed ends available upon Tmod4 deletion, which occurs during embryonic skeletal muscle development and does not require postnatal muscle use. Such a compensation mechanism appears to be a mammalian innovation, as Tmod4 deficiency leads to severe myofibril disruption and nemaline myopathy-like phenotypes in zebrafish and *Xenopus* (Berger et al., 2014; Nworu et al., 2015). The dispensability of Tmod4 for mammalian skeletal muscle development and organization also agrees with the fact that no human *TMOD4*-based nemaline myopathies have been identified to date, despite the fact that numerous nemaline myopathy-causing mutations in other thin filament structural components and actin-associated proteins have been identified (Romero et al., 2013).

Tmod regulation of thin filament lengths

Our finding that RNAi depletion of Tmod1 leads to thin filament elongation in both wild-type and Tmod4-deficient TA muscle fibers

Development (2015) 142, 4351-4362 doi:10.1242/dev.129171

provides the first direct demonstration that pointed-end capping by a sarcomeric Tmod isoform is inversely related to thin filament length in mammalian skeletal muscle fibers. Although it has been known for some time that pointed-end capping by sarcomeric Tmods is inversely related to thin filament length in cardiac myocytes as well as *Drosophila* indirect flight muscle (Bliss et al., 2014; Gregorio et al., 1995; Littlefield et al., 2001; Mardahl-Dumesnil and Fowler, 2001; Sussman et al., 1998), the only evidence for Tmod participation in thin filament length regulation in skeletal muscle has been indirect evidence obtained from dystrophic mouse muscles, in which m-calpain-induced proteolysis of Tmod1 is associated with thin filament elongation (Gokhin et al., 2014b). However, the utility of dystrophic muscles for studying Tmod-mediated thin filament length regulation is constrained by the fact that residual unproteolyzed Tmod remains in muscle after Ca^{2+} influx and m-calpain induction, and that the extent of m-calpain proteolysis is highly variable and depends on both the muscle type and the severity of the dystrophy (Gokhin et al., 2014b). Moreover, thin filament elongation in dystrophic muscle could be due to m-calpain proteolysis of non-Tmod components (Tidball and Spencer, 2000). The RNAi approach utilized here overcomes these limitations and illuminates a direct link between Tmod1-mediated capping and length regulation in both normal (wild type) and developmentally compensated (Tmod4 deficient) contexts.

In wild-type muscles, only ∼10% of filaments are capped by Tmod1 (with the remainder capped by Tmod4). Upon siRNA depletion of Tmod1 from wild-type muscles, Tmod4 now caps the pointed ends of all of the now-longer thin filaments. This is consistent with dynamic capping by Tmod4, as previously observed for Tmod1 in chick cardiac myocytes and quail skeletal myotubes (Gregorio et al., 1995; Littlefield et al., 2001; Pappas et al., 2010). In cardiac myocytes, thin filament lengths are thought to arise from competition between Tmod1 and actin subunits at pointed ends, and, thus, reduced total Tmod would be expected to allow more frequent actin subunit addition, leading to thin filament elongation (Gregorio et al., 1995; Littlefield et al., 2001). Thin filament elongation is unlikely to be due to lower affinity of Tmod4 for thin filament pointed ends compared with Tmod1, as no differences have been observed between Tmod1 and Tmod4 with respect to their actin-capping and tropomyosin-actin-capping activities (Almenar-Queralt et al., 1999). Notably, length uniformity is maintained after thin filament elongation, indicative of a constitutive mechanism for equalization of thin filament lengths across the sarcomere; such a constitutive mechanism for organelle size control has been proposed for *Chlamydomonas* flagella (Ludington et al., 2012).

Despite the compensatory upregulation of Tmod1 and normal thin filament lengths in Tmod4-deficient muscles, Tmod4-deficient muscles provide novel insights into mechanisms of Tmod-mediated regulation of actin pointed end dynamics and thin filament lengths. Unlike wild-type muscles, in which only ∼10% of filaments are capped by Tmod1, Tmod4-deficient muscles have almost all of their thin filaments capped by Tmod1. Surprisingly, regardless of these markedly different proportions of Tmod1 in wild-type and Tmod4-deficient muscles, RNAi depletion of the small amount of Tmod1 in wild-type muscle, where 90% of total Tmod remains at pointed ends, has an identical effect as depletion of Tmod1 from Tmod4-deficient muscle, where no Tmod remains at pointed ends (i.e. thin filament lengthening by ∼15% in both cases). We suggest two possibilities to explain this apparent paradox. (1) Thin filament lengths might be inversely related to sarcomeric Tmod1+4 levels, but this relationship might not be stoichiometric. Rather, any depletion of sarcomeric Tmod1+4 levels leading to uncapped pointed ends might reduce total Tmod levels below a threshold required to inhibit actin subunit association and filament lengthening. (2) Alternatively, Tmod1-deficient sarcomeres from Tmod4-deficient muscles might actually have a greater propensity for thin filament elongation owing to further reductions in total Tmod and increased actin subunit association kinetics compared with Tmod1-deficient sarcomeres from wild-type muscles; however, in this latter case, excessive elongation of uncapped thin filaments might be blocked by a structural constraint or 'ceiling' on thin filament elongation. Myosin thick filaments, titin and/or M-line components might contribute to such a ceiling, as suggested previously (Littlefield and Fowler, 1998).

Relationship between Tmods and Lmods in striated muscles

Deletion of Tmod4 with compensatory upregulation of Tmod1 during development leads to an unexpected Lmod isoform switch, with downregulation of Lmod3 and upregulation of Lmod2, suggesting the existence of a gene regulatory network mediating preferential Tmod4-Lmod3 and Tmod1-Lmod2 co-expression. Preferential Tmod4-Lmod3 and Tmod1-Lmod2 co-expression is also supported by previous findings: (1) Lmod3 is the predominant Lmod isoform in skeletal muscle, in which skeletal myofibrils contain predominantly Tmod4 on thin filament pointed ends (this study; Cenik et al., 2015); (2) Lmod2 is the predominant Lmod isoform in cardiac muscle, in which cardiac myofibrils contain solely Tmod1 on thin filament pointed ends (Chereau et al., 2008; Conley et al., 2001; Gokhin and Fowler, 2011b; Skwarek-Maruszewska et al., 2010); (3) LMOD3-deficient nemaline myopathy patients exhibit dramatic loss of TMOD4 protein (Yuen et al., 2014). Although the genetic circuitry regulating preferential Tmod4-Lmod3 and Tmod1-Lmod2 co-expression remains unknown, a possible candidate is the myocardin-related transcription factor (MRTF)/Srf pathway, which has been proposed to activate muscle-specific genes via a feedback loop initiated by Lmod3-mediated actin polymerization and depletion of soluble actin (Cenik et al., 2015). It is conceivable that co-expression of Tmod4-Lmod3 versus Tmod1-Lmod2 leads to different soluble actin levels, leading to different extents of MRTF activation and Srf and Mef2 activity, and expression of skeletal versus cardiac combinations of cytoskeletal genes.

Our unexpected observation that Lmod3 localizes ∼0.95 µm away from the Z-line in mouse skeletal muscle indicates that Lmod3 is coincident with neb-N at the junction between the nebulin-coated proximal segment and nebulin-free distal segment of the thin filament (Gokhin and Fowler, 2013). This Lmod3 localization is also similar to LMOD3 localization in some human muscle biopsies, although human LMOD3 localization is more heterogeneous and subject specific, with variable LMOD3 staining observed along the length of the filament itself, and, in a subset of instances, coinciding with both neb-N and TMOD (Yuen et al., 2014). Our co-immunoprecipitation experiments argue against the existence of Tmod-Lmod complexes, although we cannot rule out the possibility that Tmod-Lmod interactions are weak, transient and/or dependent on additional regulatory factors. Regardless, both observed Lmod3 localization patterns imply that Lmods exert at least some of their actin-regulatory effects on thin filaments by binding along filament sides. The identical positioning of Lmod3 and neb-N ∼0.95 µm away from the Z-line also agrees with the fact that both Lmod3 and neb-N are substrates of the ubiquitylation inhibitor Klhl40 (Garg et al., 2014). Lmod3/neb-N/Klhl40 interactions might constitute a novel actin-remodeling complex along the side of the thin filament, at the junction

Development (2015) 142, 4351-4362 doi:10.1242/dev.129171

between the nebulin-coated proximal segment and nebulin-free distal segment of the thin filament.

MATERIALS AND METHODS

Generation and genotyping of *Tmod4*$^{-/-}$ mice

Mouse embryonic stem cells with a *lacZ/neo* insertion in intron 2 of the *Tmod4* gene were obtained from the Knockout Mouse Project repository (project ID 33375) at the University of California-Davis and stored in liquid N_2 until use. Blastocyst injection and implantation into pseudopregnant females were performed at the Murine Genetics Core at The Scripps Research Institute. Resulting male chimeras were bred to C57BL/6J females to obtain germline transmission. Intercrosses of *Tmod4*$^{+/-}$ mice were performed to generate *Tmod4*$^{-/-}$ mice and control *Tmod4*$^{+/+}$ littermates. The presence of wild-type and mutant *Tmod4* alleles was confirmed by automated qPCR genotyping of tail-snip biopsies (Transnetyx, Cordova, TN, USA). Adult mice were sacrificed by isoflurane inhalation followed by cervical dislocation, and newborn (P0) mice were sacrificed by isoflurane inhalation followed by decapitation. All experiments were performed according to NIH animal care guidelines, as approved and enforced by the Institutional Animal Care and Use Committee at The Scripps Research Institute.

Antibodies

Primary antibodies were as follows: rabbit polyclonal antiserum to chicken Tmod4 preadsorbed by passage through a Tmod1 Sepharose column (R3577; 1:25 for cryosections, 1:2500 for western blots; Gokhin et al., 2010), affinity-purified rabbit polyclonal anti-human TMOD1 (R1749; 3.1 µg/ml for cryosections; Gokhin et al., 2010), rabbit polyclonal antiserum to residues 340-359 of a human TMOD1 peptide (PA2211; 1:5000 for western blots; Gokhin et al., 2012), rabbit polyclonal antiserum to human TMOD3 preadsorbed by passage through a Tmod1 Sepharose column (R5168; 1:100 for cryosections, 1:1000 for western blots; Gokhin et al., 2010), affinity-purified rabbit polyclonal anti-nebulin M1M2M3 domain (NEB-1; 1:100 for cryosections; Myomedix, Mannheim, Germany), affinity-purified rabbit polyclonal anti-nebulin M160-164 domain (10 µg/ml for cryosections; a gift from Carol C. Gregorio, University of Arizona, Tucson, AZ, USA), rabbit polyclonal anti-Lmod3 (14948-1-AP; 1:100 for cryosections, 1:1000 for western blots; Proteintech, Chicago, IL, USA), rabbit polyclonal anti-Lmod2 (S-12; 1:200 for western blots; Santa Cruz Biotechnology, Dallas, TX, USA), mouse monoclonal anti-Tmod1 (mAb9; 1:100 for cryosections; Gregorio et al., 1995), mouse monoclonal anti-α-actinin (EA53; 1:100 for cryosections; Sigma-Aldrich), mouse monoclonal anti-actin (C4; 1:10,000 for western blots; EMD Millipore) and mouse monoclonal anti-GAPDH (1D4; 1:5000 for western blots; Novus Biologicals). Secondary antibodies were as follows: Alexa Fluor 488-conjugated goat anti-rabbit IgG (1:200 for cryosections; Life Technologies), Alexa Fluor 647-conjugated goat anti-mouse IgG (1:200 for cryosections; Life Technologies), 800CW-conjugated goat anti-rabbit IgG (1:20,000 for western blots; LI-COR Biosciences) and 680LT-conjugated goat anti-mouse IgG (1:20,000 for western blots; LI-COR Biosciences).

Immunostaining and confocal microscopy

TA and soleus muscles were relaxed, fixed, cryosectioned and immunostained as described previously (Gokhin et al., 2014b). Alexa 488- or Alexa 647-conjugated secondary antibodies were supplemented with rhodamine-phalloidin (1:100; Life Technologies) to stain F-actin. Images of single optical sections were collected at room temperature on either a Bio-Rad Radiance 2100 laser-scanning confocal microscope mounted on a Nikon TE2000-U microscope, or on a Zeiss LSM780 laser-scanning confocal microscope mounted on a Zeiss Axio Observer.Z1 microscope. Images were acquired using 100× (1.4 NA) Plan-Apochromat oil-objective lenses with digital zoom of up to 3×. Images were processed with Volocity 6.3 (PerkinElmer), and image figures were constructed in Adobe Illustrator CS5.1.

Thin filament length measurements

DDecon was used to measure distances of sarcomeric Tmods, neb-N and Lmod3 from the Z-line as well as the breadth of the F-actin (phalloidin) signal across the Z-lines of adjacent half-sarcomeres (I-Z-I arrays) using line-scans of fluorescence images, as described previously (Gokhin et al., 2012; Littlefield and Fowler, 2002). Tmod distances were determined from Tmod1 and Tmod4 localization in *Tmod4*$^{+/+}$ muscles or just Tmod1 localization in *Tmod4*$^{-/-}$ muscles. DDecon was performed using an open-source ImageJ plugin (available at http://www.scripps.edu/fowler/ddecon/). Distances were calculated by converting pixel sizes into µm.

Histology

Transverse sections of TA, EDL and soleus muscles were subjected to Haematoxylin and Eosin (H&E) and Gömöri trichrome staining. Images were collected on a Zeiss Axioskop bright-field microscope using a 10× (0.45 NA) air-objective lens (zoom=2) and a Zeiss Axiocam CCD camera at RT. Centrally nucleated fibers were manually counted in H&E-stained images. Fiber cross-sectional area was determined by manual segmentation of fibers and converting enclosed pixel areas into µm^2.

Transmission electron microscopy

Mice were perfusion fixed in 4% paraformaldehyde +1.5% glutaraldehyde in 0.1 M cacodylate buffer, and TA and EDL muscles were processed for transmission electron microscopy as described previously (Gokhin et al., 2010). Sections (60 nm thin) were cut, mounted on copper slot grids coated with parlodion, stained with uranyl acetate and lead citrate, and examined on a Philips CM100 transmission electron microscope at 80 kV.

Co-immunoprecipitation

Co-immunoprecipitation was performed as described previously (Gokhin and Fowler, 2011a). Briefly, mouse TA and EDL muscles were homogenized in RIPA buffer supplemented with protease inhibitor cocktail (1:1000) and centrifuged at 10,000 ***g***. The resulting supernatant was divided into 1-ml aliquots, to which one of the following was added: 2 µg rabbit polyclonal anti-Tmod4 (R3577), 2 µg rabbit polyclonal anti-human Tmod1 (R1749) or 2 µg of preimmune control IgG. Antibody-bound complexes were adsorbed to 100 µl µMACS Protein A-conjugated superparamagnetic MicroBeads (Miltenyi Biotec) and incubated for 1 h on ice, followed by passage through a µColumn (Miltenyi Biotec) using a µMACS magnetic separator (Miltenyi Biotec). Beads were washed with RIPA buffer and eluted with 100 µl of 1× SDS sample buffer. The input extract (diluted in 2× SDS sample buffer) and eluted immunoprecipitates were then subjected to SDS-PAGE and western blotting, as described below.

Gel sample preparation and western blotting

For western blots of whole-muscle homogenates, TA, EDL, soleus, diaphragm, and neonatal leg and flank muscles were dissected in ice-cold PBS and homogenized with a Tekmar Tissumizer in ten volumes of PBS supplemented with protease inhibitor cocktail (1:1000). Protein standards for quantitative western blotting were prepared as described previously (Gokhin et al., 2014b). First, protein standards for SDS-PAGE and Coomassie Blue staining to determine actin concentrations in isolated myofibrils were prepared from rabbit skeletal muscle actin (Cytoskeleton, Denver, CO, USA). Second, protein standards for quantitative western blots were prepared by spiking increasing volumes of *Tmod1*$^{-/-}$ (Gokhin et al., 2010) or *Tmod4*$^{-/-}$ TA muscle homogenates with increasing amounts of recombinant purified human Tmod1 or mouse Tmod4 proteins (Yamashiro et al., 2010), respectively. This approach equalized the effects of endogenous non-Tmod proteins on the differential western transfer efficiencies of endogenous versus recombinant purified Tmods, as described previously (Gokhin et al., 2014b).

All protein preparations were solubilized in equal volumes of 2× SDS sample buffer and boiled for 5 min. SDS-PAGE, transfer to nitrocellulose, blocking, and antibody incubations were performed as described previously (Gokhin et al., 2014b). Bands were visualized using a LI-COR Odyssey infrared imaging system, and background-corrected band intensities were densitometrically quantified in ImageJ. Where appropriate, band intensities were normalized to Gapdh to control for loading.

MHC isoform composition

Gel samples of whole-muscle homogenates were prepared as described for western blotting. Proteins were then separated by SDS-PAGE on 8% Tris-

Development (2015) 142, 4351-4362 doi:10.1242/dev.129171

glycine mini-gels, as described previously (Talmadge and Roy, 1993). SDS-PAGE was performed for 16 h at 140 V. The upper tank buffer was supplemented with 1 mM dithiothreitol, and the lower tank buffer was one-sixth the concentration of the upper tank buffer (Kohn and Myburgh, 2006). Gels were silver-stained, and background-corrected intensities of type-1, -2A, -2X and -2B MHC bands were densitometrically quantified in ImageJ.

Skinned muscle fiber mechanics

Physiological measurement of specific force production, rate constant of force redevelopment after unloaded sarcomere shortening (k_{tr}), thin filament Ca^{2+} sensitivity (pCa_{50}), and cooperativity of thin filament activation [Hill coefficient (n_H)] using skinned, Ca^{2+}-activated TA muscle fibers was performed as described previously (Ochala et al., 2014).

RNA sequencing

RNA sequencing was performed as described previously (Christodoulou et al., 2011). Briefly, an RNA sequencing library was constructed by random hexamer priming of mRNA pooled from three biological replicates of wild-type mouse TA, soleus, diaphragm and left ventricular muscles (Domenighetti et al., 2014). The resulting cDNA library was uniformly amplified to subsaturating levels. Alignment of reads was performed using TopHat 1.0.14 (Trapnell et al., 2009). Read-depth profiles were constructed using TopHat's 'wiggles' tool, and values were normalized to total aligned reads and uploaded onto the University of California-Santa Cruz Genome Browser (http://genome.ucsc.edu). RNA sequencing data have been deposited in Gene Expression Omnibus under accession number GSE75318.

qRT-PCR

Total RNA was extracted from skeletal muscle tissues with TRIzol reagent (Life Technologies) and reverse-transcribed into cDNA using SuperScript III Reverse Transcriptase with random hexamer primers (Life Technologies), according to the manufacturer's instructions. cDNA was analyzed using a Bio-Rad iCycler iQ apparatus, with each reaction containing 60 ng cDNA as template, LightCycler 480 SYBR Green I Master (Roche), and the following gene-specific primers (Integrated DNA Technologies): *Tmod4* forward, 5′-GATGCGGTAGAGATGGAGATG-3′; *Tmod4* reverse, 5′-TCTCTTCTTTTGCTGACGACG-3′; *Tmod1* forward, 5′-CAACGCCATGATGAGCAAC-3′; *Tmod1* reverse, 5′-CATCGGTAG-AACACGTCCAG-3′; *Lmod3* forward, 5′-CCGCTGGTGGAAATCACT-CCC-3′; *Lmod3* reverse, 5′-ACTCCAGCTCCTTTGGCAGTTGC-3′; *Lmod2* forward, 5′-TTGGAGAAGGAACGGCTGGG-3′; *Lmod2* reverse, 5′-CCTCAGAGACTTCGCTGTTGCTCTC-3′; *Gapdh* forward, 5′-ACC-ACAGTCCATGCCATCAC-3′; *Gapdh* reverse, 5′-TCCACCACCCTGT-TGCTGTA-3′. *Tmod4* and *Tmod1* primers (Gokhin et al., 2014b) and *Lmod3* and *Lmod2* primers (Cenik et al., 2015) were as previously published, and *Gapdh* primers were ReadyMade primers from Integrated DNA Technologies. Relative gene expression levels were calculated as $2^{-\Delta\Delta Ct}$ with normalization to *Gapdh*, as described previously (Livak and Schmittgen, 2001).

In vivo RNAi

Mice were anesthetized with isoflurane (4% for induction, 2% for maintenance) with 1 liter/min O_2, until cessation of the toe-pinch withdrawal reflex was attained. One nmol siRNA and Lipofectamine RNAiMAX transfection reagent (1:100, Life Technologies) were diluted to a final volume of 10 µl, drawn into a 25-gauge syringe needle, and slowly injected into the midbelly of the TA muscle. Two different Silencer Select siRNA constructs (Life Technologies) were used to knock down Tmod1: siTmod1a forward, 5′-CUAGAAGAGGUUAAUCUUATT-3′; siTmod1a reverse, 5′-UAAGAUUAACCUCUUCUAGTT-3′; siTmod1b forward, 5′-GCUGAAAUGCUGAAAGUGATT-3′; siTmod1b reverse, 5′-UCACUUUCAGCAUUUCAGCAA-3′. As a negative control, a Stealth RNAi negative control duplex (Life Technologies) was used and is referred to as siScr. After injection, the ankle joint was passively dorsi- and plantarflexed to facilitate distribution of injectate throughout the TA, and mice were removed from anesthesia and allowed to recover on a heated pad. After 1 week, TA muscles were excised and processed for immunostaining and confocal microscopy, as described above.

Statistics

Data are presented as either mean±s.d. or mean±s.e.m., where appropriate. Differences between groups were detected using Student's *t*-test or one-way ANOVA with post hoc Fisher's LSD tests, where appropriate. Statistical significance was defined as $P<0.05$. Analysis was performed in Microsoft Excel.

Acknowledgements

We gratefully acknowledge Anita Sansoucie for assistance with histology, Malcolm Wood for assistance with transmission electron microscopy, Roberta Nowak for assistance with mouse breeding, and Jonathan and Christine (Kricket) Seidman for access to their muscle RNA-seq library.

Competing interests

The authors declare no competing or financial interests.

Author contributions

D.S.G. and V.M.F. conceived the study and designed the experiments. D.S.G., J.O. and A.A.D. performed the experiments and analyzed data. D.S.G. prepared the figures and wrote the paper with assistance from the other authors.

Funding

This work was supported by a development grant from the Muscular Dystrophy Association [234106 to D.S.G.]; a National Institutes of Health (NIH) National Institute of Arthritis and Musculoskeletal and Skin Diseases (NIAMS) Pathway to Independence award [K99-AR066534 to D.S.G.]; a Medical Research Council NI grant [MR/N002768/1 to J.O.]; an NIH National Heart, Lung, and Blood Institute grant [R01-HL083464 to V.M.F.]; and an NIH NIAMS grant to the Imaging Core of the San Diego Skeletal Muscle Research Center [P30-AR061303to V.M.F.]. Deposited in PMC for release after 6 months.

Supplementary information

Supplementary information available online at
http://dev.biologists.org/lookup/suppl/doi:10.1242/dev.129171/-/DC1

References

Almenar-Queralt, A., Lee, A., Conley, C. A., de Pouplana, L. R. and Fowler, V. M. (1999). Identification of a novel tropomodulin isoform, skeletal tropomodulin, that caps actin filament pointed ends in fast skeletal muscle. *J. Biol. Chem.* **274**, 28466-28475.

Bang, M.-L., Li, X., Littlefield, R., Bremner, S., Thor, A., Knowlton, K. U., Lieber, R. L. and Chen, J. (2006). Nebulin-deficient mice exhibit shorter thin filament lengths and reduced contractile function in skeletal muscle. *J. Cell Biol.* **173**, 905-916.

Berger, J., Tarakci, H., Berger, S., Li, M., Hall, T. E., Arner, A. and Currie, P. D. (2014). Loss of Tropomodulin4 in the zebrafish mutant trage causes cytoplasmic rod formation and muscle weakness reminiscent of nemaline myopathy. *Dis. Model. Mech.* **7**, 1407-1415.

Bliss, K. T., Tsukada, T., Novak, S. M., Dorovkov, M. V., Shah, S. P., Nworu, C., Kostyukova, A. S. and Gregorio, C. C. (2014). Phosphorylation of tropomodulin1 contributes to the regulation of actin filament architecture in cardiac muscle. *FASEB J.* **28**, 3987-3995.

Castillo, A., Nowak, R., Littlefield, K. P., Fowler, V. M. and Littlefield, R. S. (2009). A nebulin ruler does not dictate thin filament lengths. *Biophys. J.* **96**, 1856-1865.

Cenik, B. K., Garg, A., McAnally, J. R., Shelton, J. M., Richardson, J. A., Bassel-Duby, R., Olson, E. N. and Liu, N. (2015). Severe myopathy in mice lacking the MEF2/SRF-dependent gene leiomodin-3. *J. Clin. Invest.* **125**, 1569-1578.

Chandra, M., Mamidi, R., Ford, S., Hidalgo, C., Witt, C., Ottenheijm, C., Labeit, S. and Granzier, H. (2009). Nebulin alters cross-bridge cycling kinetics and increases thin filament activation: a novel mechanism for increasing tension and reducing tension cost. *J. Biol. Chem.* **284**, 30889-30896.

Chereau, D., Boczkowska, M., Skwarek-Maruszewska, A., Fujiwara, I., Hayes, D. B., Rebowski, G., Lappalainen, P., Pollard, T. D. and Dominguez, R. (2008). Leiomodin is an actin filament nucleator in muscle cells. *Science* **320**, 239-243.

Christodoulou, D. C., Gorham, J. M., Herman, D. S. and Seidman, J. G. (2011). Construction of normalized RNA-seq libraries for next-generation sequencing using the crab duplex-specific nuclease. *Curr. Protoc. Mol. Biol.* Chapter 4, Unit4. 12.

Conley, C. A., Fritz-Six, K. L., Almenar-Queralt, A. and Fowler, V. M. (2001). Leiomodins: larger members of the tropomodulin (Tmod) gene family. *Genomics* **73**, 127-139.

Cox, P. R., Fowler, V., Xu, B., Sweatt, J. D., Paylor, R. and Zoghbi, H. Y. (2003). Mice lacking Tropomodulin-2 show enhanced long-term potentiation, hyperactivity, and deficits in learning and memory. *Mol. Cell. Neurosci.* **23**, 1-12.

Domenighetti, A. A., Chu, P.-H., Wu, T., Sheikh, F., Gokhin, D. S., Guo, L. T., Cui, Z., Peter, A. K., Christodoulou, D. C., Parfenov, M. G. et al. (2014). Loss of

FHL1 induces an age-dependent skeletal muscle myopathy associated with myofibrillar and intermyofibrillar disorganization in mice. *Hum. Mol. Genet.* **23**, 209-225.

Fowler, V. M., Sussmann, M. A., Miller, P. G., Flucher, B. E. and Daniels, M. P. (1993). Tropomodulin is associated with the free (pointed) ends of the thin filaments in rat skeletal muscle. *J. Cell Biol.* **120**, 411-420.

Garg, A., O'Rourke, J., Long, C., Doering, J., Ravenscroft, G., Bezprozvannaya, S., Nelson, B. R., Beetz, N., Li, L., Chen, S. et al. (2014). KLHL40 deficiency destabilizes thin filament proteins and promotes nemaline myopathy. *J. Clin. Invest.* **124**, 3529-3539.

Gokhin, D. S. and Fowler, V. M. (2011a). Cytoplasmic gamma-actin and tropomodulin isoforms link to the sarcoplasmic reticulum in skeletal muscle fibers. *J. Cell Biol.* **194**, 105-120.

Gokhin, D. S. and Fowler, V. M. (2011b). Tropomodulin capping of actin filaments in striated muscle development and physiology. *J. Biomed. Biotechnol.* **2011**, 103069.

Gokhin, D. S. and Fowler, V. M. (2013). A two-segment model for thin filament architecture in skeletal muscle. *Nat. Rev. Mol. Cell Biol.* **14**, 113-119.

Gokhin, D. S., Lewis, R. A., McKeown, C. R., Nowak, R. B., Kim, N. E., Littlefield, R. S., Lieber, R. L. and Fowler, V. M. (2010). Tropomodulin isoforms regulate thin filament pointed-end capping and skeletal muscle physiology. *J. Cell Biol.* **189**, 95-109.

Gokhin, D. S., Kim, N. E., Lewis, S. A., Hoenecke, H. R., D'Lima, D. D. and Fowler, V. M. (2012). Thin-filament length correlates with fiber type in human skeletal muscle. *Am. J. Physiol. Cell Physiol.* **302**, C555-C565.

Gokhin, D. S., Dubuc, E. A., Lian, K. Q., Peters, L. L. and Fowler, V. M. (2014a). Alterations in thin filament length during postnatal skeletal muscle development and aging in mice. *Front. Physiol.* **5**, 399.

Gokhin, D. S., Tierney, M. T., Sui, Z., Sacco, A. and Fowler, V. M. (2014b). Calpain-mediated proteolysis of tropomodulin isoforms leads to thin filament elongation in dystrophic skeletal muscle. *Mol. Biol. Cell* **25**, 852-865.

Granzier, H. L., Akster, H. A. and Ter Keurs, H. E. (1991). Effect of thin filament length on the force-sarcomere length relation of skeletal muscle. *Am. J. Physiol.* **260**, C1060-C1070.

Gregorio, C. C., Weber, A., Bondad, M., Pennise, C. R. and Fowler, V. M. (1995). Requirement of pointed-end capping by tropomodulin to maintain actin filament length in embryonic chick cardiac myocytes. *Nature* **377**, 83-86.

Hanft, L. M., Rybakova, I. N., Patel, J. R., Rafael-Fortney, J. A. and Ervasti, J. M. (2006). Cytoplasmic gamma-actin contributes to a compensatory remodeling response in dystrophin-deficient muscle. *Proc. Natl. Acad. Sci. USA* **103**, 5385-5390.

Kohn, T. A. and Myburgh, K. H. (2006). Electrophoretic separation of human skeletal muscle myosin heavy chain isoforms: the importance of reducing agents. *J. Physiol. Sci.* **56**, 355-360.

Lieber, R. L. (2002). *Skeletal Muscle Structure, Function, and Plasticity: The Physiological Basis of Rehabilitation*. Philadelphia: Lippincott Williams & Wilkins.

Littlefield, R. and Fowler, V. M. (1998). Defining actin filament length in striated muscle: rulers and caps or dynamic stability? *Annu. Rev. Cell Dev. Biol.* **14**, 487-525.

Littlefield, R. and Fowler, V. M. (2002). Measurement of thin filament lengths by distributed deconvolution analysis of fluorescence images. *Biophys. J.* **82**, 2548-2564.

Littlefield, R. S. and Fowler, V. M. (2008). Thin filament length regulation in striated muscle sarcomeres: pointed-end dynamics go beyond a nebulin ruler. *Semin. Cell Dev. Biol.* **19**, 511-519.

Littlefield, R., Almenar-Queralt, A. and Fowler, V. M. (2001). Actin dynamics at pointed ends regulates thin filament length in striated muscle. *Nat. Cell Biol.* **3**, 544-551.

Livak, K. J. and Schmittgen, T. D. (2001). Analysis of relative gene expression data using real-time quantitative PCR and the 2(-Delta Delta C(T)) Method. *Methods* **25**, 402-408.

Ludington, W. B., Shi, L. Z., Zhu, Q., Berns, M. W. and Marshall, W. F. (2012). Organelle size equalization by a constitutive process. *Curr. Biol.* **22**, 2173-2179.

Mardahl-Dumesnil, M. and Fowler, V. M. (2001). Thin filaments elongate from their pointed ends during myofibril assembly in Drosophila indirect flight muscle. *J. Cell Biol.* **155**, 1043-1054.

Moyer, J. D., Nowak, R. B., Kim, N. E., Larkin, S. K., Peters, L. L., Hartwig, J., Kuypers, F. A. and Fowler, V. M. (2010). Tropomodulin 1-null mice have a mild spherocytic elliptocytosis with appearance of tropomodulin 3 in red blood cells and disruption of the membrane skeleton. *Blood* **116**, 2590-2599.

Mudry, R. E., Perry, C. N., Richards, M., Fowler, V. M. and Gregorio, C. C. (2003). The interaction of tropomodulin with tropomyosin stabilizes thin filaments in cardiac myocytes. *J. Cell Biol.* **162**, 1057-1068.

Nanda, V. and Miano, J. M. (2012). Leiomodin 1, a new serum response factor-dependent target gene expressed preferentially in differentiated smooth muscle cells. *J. Biol. Chem.* **287**, 2459-2467.

Nworu, C. U., Kraft, R., Schnurr, D. C., Gregorio, C. C. and Krieg, P. A. (2015). Leiomodin 3 and tropomodulin 4 have overlapping functions during skeletal myofibrillogenesis. *J. Cell Sci.* **128**, 239-250.

Ochala, J., Gokhin, D. S., Pénisson-Besnier, I., Quijano-Roy, S., Monnier, N., Lunardi, J., Romero, N. B. and Fowler, V. M. (2012). Congenital myopathy-causing tropomyosin mutations induce thin filament dysfunction via distinct physiological mechanisms. *Hum. Mol. Genet.* **21**, 4473-4485.

Ochala, J., Gokhin, D. S., Iwamoto, H. and Fowler, V. M. (2014). Pointed-end capping by tropomodulin modulates actomyosin crossbridge formation in skeletal muscle fibers. *FASEB J.* **28**, 408-415.

Olson, E. N. and Nordheim, A. (2010). Linking actin dynamics and gene transcription to drive cellular motile functions. *Nat. Rev. Mol. Cell Biol.* **11**, 353-365.

Ottenheijm, C. A. C., Witt, C. C., Stienen, G. J., Labeit, S., Beggs, A. H. and Granzier, H. (2009). Thin filament length dysregulation contributes to muscle weakness in nemaline myopathy patients with nebulin deficiency. *Hum. Mol. Genet.* **18**, 2359-2369.

Ottenheijm, C. A. C., Hooijman, P., DeChene, E. T., Stienen, G. J., Beggs, A. H. and Granzier, H. (2010). Altered myofilament function depresses force generation in patients with nebulin-based nemaline myopathy (NEM2). *J. Struct. Biol.* **170**, 334-343.

Ottenheijm, C. A. C., Buck, D., de Winter, J. M., Ferrara, C., Piroddi, N., Tesi, C., Jasper, J. R., Malik, F. I., Meng, H., Stienen, G. J. M. et al. (2013). Deleting exon 55 from the nebulin gene induces severe muscle weakness in a mouse model for nemaline myopathy. *Brain* **136**, 1718-1731.

Pappas, C. T., Bhattacharya, N., Cooper, J. A. and Gregorio, C. C. (2008). Nebulin interacts with CapZ and regulates thin filament architecture within the Z-disc. *Mol. Biol. Cell* **19**, 1837-1847.

Pappas, C. T., Krieg, P. A. and Gregorio, C. C. (2010). Nebulin regulates actin filament lengths by a stabilization mechanism. *J. Cell Biol.* **189**, 859-870.

Pappas, C. T., Bliss, K. T., Zieseniss, A. and Gregorio, C. C. (2011). The nebulin family: an actin support group. *Trends Cell Biol.* **21**, 29-37.

Pappas, C. T., Mayfield, R. M., Henderson, C., Jamilpour, N., Cover, C., Hernandez, Z., Hutchinson, K. R., Chu, M., Nam, K. H., Valdez, J. M. et al. (2015). Knockout of Lmod2 results in shorter thin filaments followed by dilated cardiomyopathy and juvenile lethality. *Proc. Natl. Acad. Sci. USA* **112**, 13573-13578.

Pette, D. and Staron, R. S. (1990). Cellular and molecular diversities of mammalian skeletal muscle fibers. *Rev. Physiol. Biochem. Pharmacol.* **116**, 1-76.

Ringkob, T. P., Swartz, D. R. and Greaser, M. L. (2004). Light microscopy and image analysis of thin filament lengths utilizing dual probes on beef, chicken, and rabbit myofibrils. *J. Anim. Sci.* **82**, 1445-1453.

Romero, N. B., Sandaradura, S. A. and Clarke, N. F. (2013). Recent advances in nemaline myopathy. *Curr. Opin. Neurol.* **26**, 519-526.

Schiaffino, S. and Reggiani, C. (1996). Molecular diversity of myofibrillar proteins: gene regulation and functional significance. *Physiol. Rev.* **76**, 371-423.

Skwarek-Maruszewska, A., Boczkowska, M., Zajac, A. L., Kremneva, E., Svitkina, T., Dominguez, R. and Lappalainen, P. (2010). Different localizations and cellular behaviors of leiomodin and tropomodulin in mature cardiomyocyte sarcomeres. *Mol. Biol. Cell* **21**, 3352-3361.

Sussman, M. A., Baque, S., Uhm, C.-S., Daniels, M. P., Price, R. L., Simpson, D., Terracio, L. and Kedes, L. (1998). Altered expression of tropomodulin in cardiomyocytes disrupts the sarcomeric structure of myofibrils. *Circ. Res.* **82**, 94-105.

Talmadge, R. J. and Roy, R. R. (1993). Electrophoretic separation of rat skeletal muscle myosin heavy-chain isoforms. *J. Appl. Physiol.* **75**, 2337-2340.

Tian, L., Ding, S., You, Y., Li, T.-r., Liu, Y., Wu, X., Sun, L. and Xu, T. (2015). Leiomodin-3-deficient mice display nemaline myopathy with fast-myofiber atrophy. *Dis. Model. Mech.* **8**, 635-641.

Tidball, J. G. and Spencer, M. J. (2000). Calpains and muscular dystrophies. *Int. J. Biochem. Cell Biol.* **32**, 1-5.

Trapnell, C., Pachter, L. and Salzberg, S. L. (2009). TopHat: discovering splice junctions with RNA-Seq. *Bioinformatics* **25**, 1105-1111.

Tsukada, T., Pappas, C. T., Moroz, N., Antin, P. B., Kostyukova, A. S. and Gregorio, C. C. (2010). Leiomodin-2 is an antagonist of tropomodulin-1 at the pointed end of the thin filaments in cardiac muscle. *J. Cell Sci.* **123**, 3136-3145.

Watakabe, A., Kobayashi, R. and Helfman, D. M. (1996). N-tropomodulin: a novel isoform of tropomodulin identified as the major binding protein to brain tropomyosin. *J. Cell Sci.* **109**, 2299-2310.

Yamashiro, S., Speicher, K. D., Speicher, D. W. and Fowler, V. M. (2010). Mammalian tropomodulins nucleate actin polymerization via their actin monomer binding and filament pointed end-capping activities. *J. Biol. Chem.* **285**, 33265-33280.

Yamashiro, S., Gokhin, D. S., Kimura, S., Nowak, R. B. and Fowler, V. M. (2012). Tropomodulins: pointed-end capping proteins that regulate actin filament architecture in diverse cell types. *Cytoskeleton* **69**, 337-370.

Yuen, M., Sandaradura, S. A., Dowling, J. J., Kostyukova, A. S., Moroz, N., Quinlan, K. G., Lehtokari, V.-L., Ravenscroft, G., Todd, E. J., Ceyhan-Birsoy, O. et al. (2014). Leiomodin-3 dysfunction results in thin filament disorganization and nemaline myopathy. *J. Clin. Invest.* **124**, 4693-4708.

SUPPLEMENTARY FIGURES

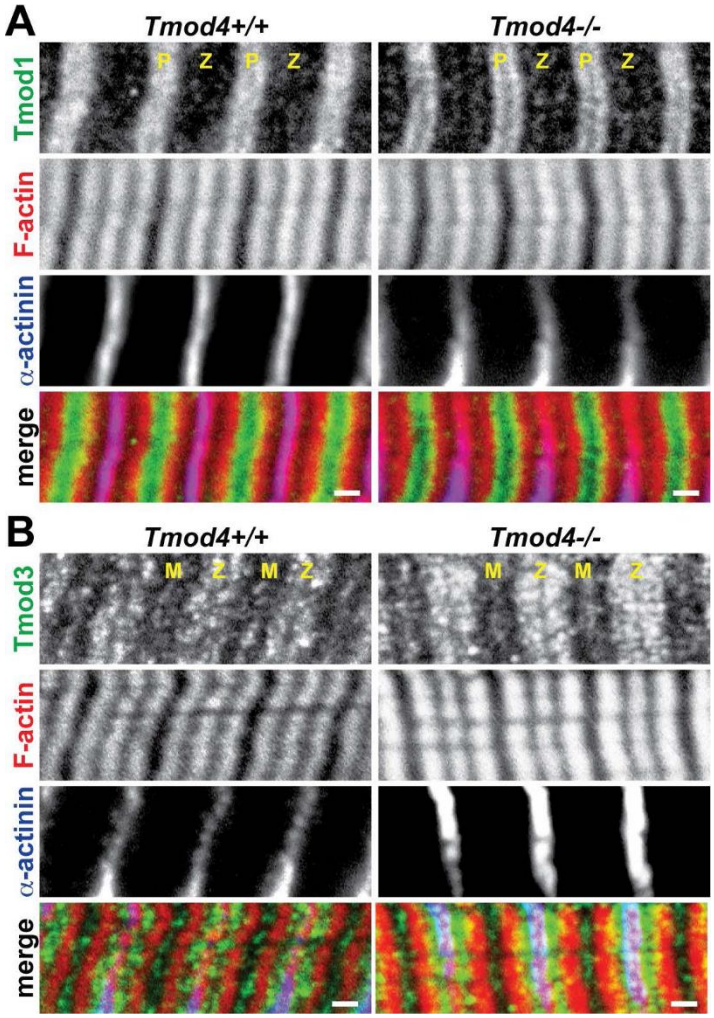

Supplementary Figure 1. Deletion of Tmod4 does not impact myofibril organization in soleus muscle. (A-B) Longitudinal cryosections of soleus muscles from 2-mo-old *Tmod4*$^{+/+}$ and *Tmod4*$^{-/-}$ mice were immunostained for either (A) Tmod1 or (B) Tmod3, immunostained for α-actinin, and phalloidin-stained for F-actin. Note that increased Tmod1 protein levels in *Tmod4*$^{-/-}$ soleus muscle determined by western blotting (Fig. 3E) are not consistently measurable by immunofluorescence and confocal microscopy. P, thin filament pointed ends; Z, Z-line; M, M-line. Bars, 1 μm.

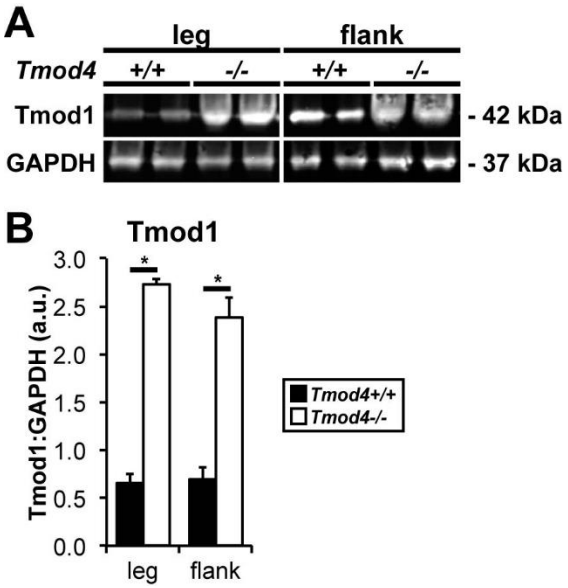

Supplementary Figure 2. Deletion of Tmod4 induces a compensatory increase in Tmod1 protein levels in neonatal skeletal muscle. (A) Western blots of homogenates of leg and flank muscles from newborn (P0) *Tmod4*$^{+/+}$ and *Tmod4*$^{-/-}$ mice were probed using an anti-Tmod1 antibody. GAPDH was used as a loading control. (B) Quantification of western blots. Error bars reflect mean±s.e.m. of n=3 lanes/genotype within a single blot.

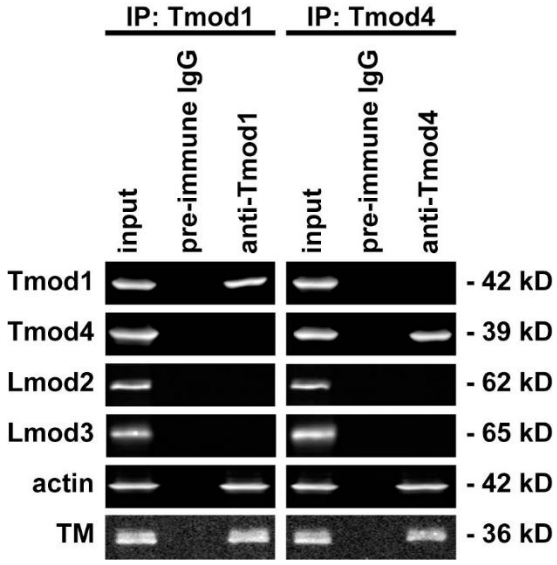

Supplementary Figure 3. Tmod1 and Tmod4 do not coimmunoprecipitate with Lmod2 or Lmod3. Shown are western blots of supernatants of RIPA buffer-extracted muscle lysates coimmunoprecipitated using anti-Tmod1- or anti-Tmod4-coated beads. Input extract was used as a positive control, and beads coated with pre-immune IgG were used as a negative control. Note coimmunoprecipitation of Tmod1 and Tmod4 with actin and α/βTM but neither Lmod2 nor Lmod3.

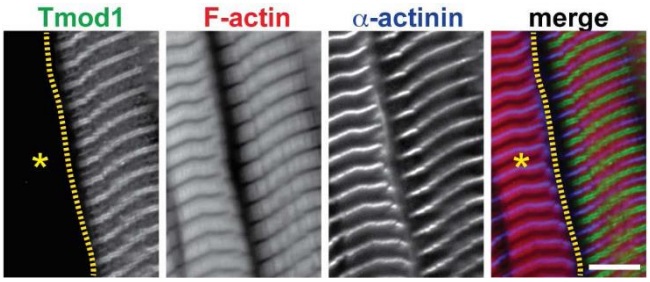

Supplementary Figure 4. Sample low-magnification image of Tmod1-positive and Tmod1-negative muscle fibers coexisting within an siTmod1a-injected muscle. A TA muscle from a 2-mo-old *Tmod4*$^{+/+}$ mouse was injected with siTmod1a and excised 1 week post-injection. Shown is a longitudinal cryosection immunostained for either immunostained for Tmod1 and α-actinin, and phalloidin-stained for F-actin. Yellow asterisk indicates a Tmod1-negative fiber; dotted yellow line indicates the periphery of the Tmod1-negative fiber. Bar, 7 μm.

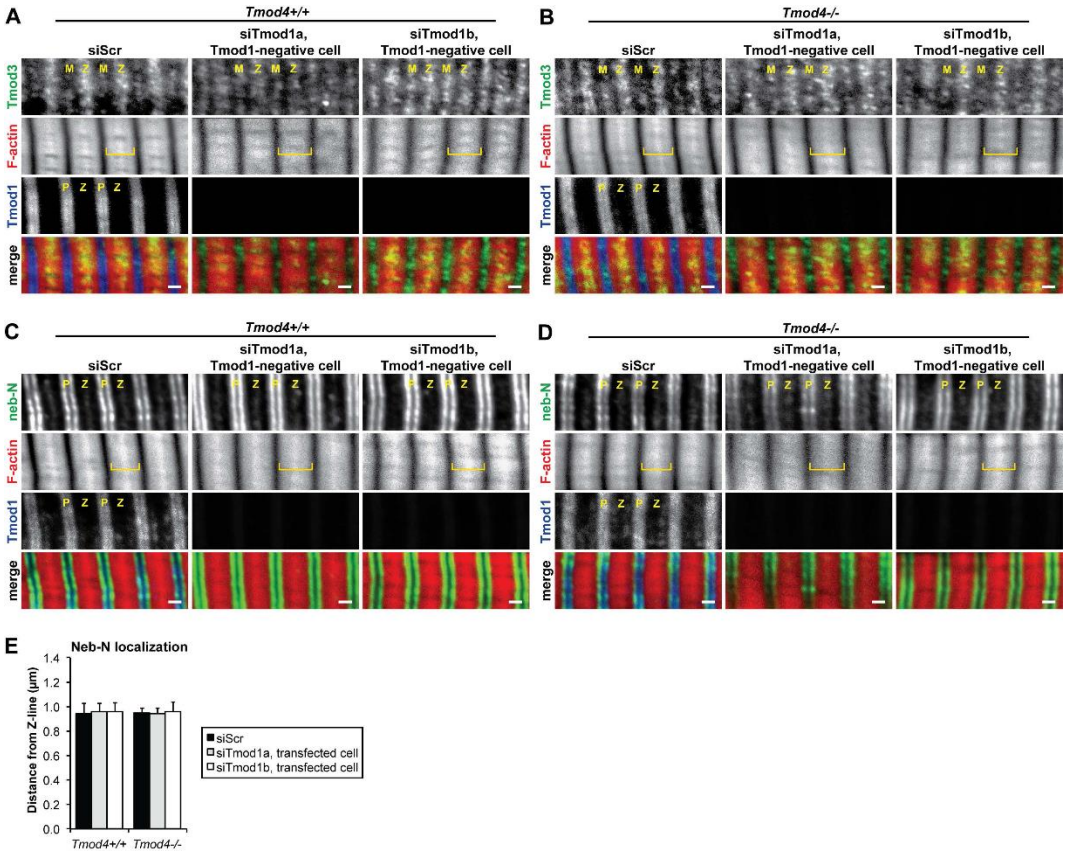

Supplementary Figure 5. RNAi knockdown of Tmod1 from *Tmod4*$^{+/+}$ or *Tmod4*$^{-/-}$ muscles does not affect the localization of Tmod3 or neb-N. (A-D) TA muscles from 2-mo-old (A,C) *Tmod4*$^{+/+}$ and (B,D) *Tmod4*$^{-/-}$ mice were injected with siScr, siTmod1a, or siTmod1b and excised 1 week post-injection. Shown are longitudinal cryosections immunostained for either (A,B) Tmod3 or (C,D) neb-N, immunostained for Tmod1, and phalloidin-stained for F-actin. Yellow brackets signify thin filament arrays (I-Z-I regions) that widen after Tmod1 knockdown. P, thin filament pointed ends; Z, Z-line; M, M-line. Bars, 1 μm. (E) Distance of neb-N from the Z-line in TA muscles from 2-mo-old *Tmod4*$^{+/+}$ and *Tmod4*$^{-/-}$ mice injected with siScr, siTmod1a, or siTmod1b, determined using DDecon analysis of fluorescence images. Error bars reflect mean±s.d. of n=50 myofibrils/genotype randomly selected from n=3-4 muscles/genotype.